3-29-2020

Novel Photon-Detector Models for Enhanced Quantum Information Processing

Elisha Siddiqui

NOVEL PHOTON-DETECTOR MODELS FOR ENHANCED QUANTUM INFORMATION PROCESSING

A Dissertation

Submitted to the Graduate Faculty of the
Louisiana State University and
Agricultural and Mechanical College
in Partial Fulfillment of the
requirements for the Degree of
Doctor of Philosophy

in

The Department of Physics and Astronomy

by
Elisha Siddiqui
B.S., Delhi University, 2011
M.S., Jawaharlal Nehru University, 2013
M.S., Louisiana State University, 2016
May 2020

To my Savior and Lord Jesus without whom I could never make it.

To my parents who have loved me and provided for me lavishly.

To my love Augustus who has never given up on me and walked with me through this Ph.D, cheering me on the way.

ACKNOWLEDGEMENTS

First and foremost all Glory and praise to my Lord and Savior Jesus who has made it possible for me to complete this Ph.D. I am reminded of Psalm 34, for I indeed sought the Lord and He answered me. Those who look on Him are radiant, they will never be ashamed. The Lord has supplied my every need during this Ph.D, I can say without a doubt that I have lacked nothing for my Lord has provided for me.

I am extremely thankful to my thesis advisors Dr. Jonathan P. Dowling and Dr. Hwang Lee. I am so grateful to Jon for always showing concern not just for me but for all his students. I can say without a doubt that Jon is one of those few supervisors who genuinely cares for his students. Jon has given me the freedom in research, and allowed me to express myself. He constantly speaks encouraging words over me and has bolstered my confidence. He always provides insight and help whenever I am stuck on a problem. Jon has managed to create a stress free work environment, not compromising on productivity but making research enjoyable as it should be. I will forever remember this quote from him ïf it is too hard for others, it is just the right problem for usëspecially when I am afraid of tackling a problem. I also thank Jon for giving me the opportunity to travel for research to China and Israel. I will forever remember the research experiences I've had at New York University, Shanghai, Hebrew university of Jerusalem, and Weizmann institute of Physics, Rehovat.

I also want to express my gratitude to Dr. Lee for always being there! No matter how busy he is, Dr. Lee has always taken out time to have research discussions with me. He listens patiently and carefully to me when I am stuck on a problem. He always provides the fresh outlook to a problem and has been instrumental in me getting breakthroughs on several of my research projects. On days when I was discouraged and down, Dr. Lee encouraged me and made sure I was not too hard on myself.

I thank the other members of my committee, Thomas Corbitt, Warren Johnson, and dean's representative Guoli Ding, for offering their time and input to my work.

I want to say thank you to Lior Cohen, who added that spice into my research life. His hard-working nature, and the passion for Physics is inspirational. Through all the noisy arguments, we learnt something and I thank him for that.

I would like to mention Carol Duran for being a part of this long journey of Ph.D. and taking care of me when I needed it.

Also I want to say thank you to all my teachers over the years who have taught me and impact my life in one way or the other, in particular my gratitude to Dr. Abhinav Gupta, who taught me quantum mechanics during my undergraduate in Physics. What I learnt from him in that year long course, helped me to catch up quickly on quantum optics.

Also, I want to thank Ms. Jennifer Zimmerman, for being my best friend, my mentor and prayer partner. Thank you for always encouraging me and praying for me. I love you so much.

Special thanks to my choir family at CBC, for teaching me so much about community, and of course music. It was perfect stress buster to sing praises to our Lord together. Thank you to my friends at the chapel, some who have left especially Liz, and who are still here. Your prayers are greatly appreciated.

Lastly, I want to say thank you to my beloved, my husband Augustus who I love so much. You are a blessing to me and a gift from Above. You have walked through difficult seasons of my life, and silently borne some of my outbursts during the whole process of completing this Ph.D. You have taught me so much about life, to keep going and be strong and courageous in the Lord. No matter how I felt during this journey, your love has been a blessing.

Thank you to my parents for their love and support, and those back home who have prayed for me, and invested in my life so I could achieve this Ph.D.

TABLE OF CONTENTS

ABSTRACT

This work is devoted to the development of novel photon-detector models at room temperature using quantum optics elements. This work comprises of two photon-number-resolving detector (PNRD) models, and the application of PNRD in LIDAR.

The first model is based on using a two-mode squeezing device to resolve photon number at room temperature. In this model we study the average intensity-intensity correlations signal at the output of a two-mode squeezing device with $|N\rangle \bigotimes |\alpha\rangle$ as the two input modes. We show that the input photon-number can be resolved from the average intensity-intensity correlations. In particular, we show jumps in the average intensity-intensity correlations signal as a function of input photon-number N. Therefore, we propose that such a device may be deployed as photon-number-resolving detector at room temperature with high efficiency.

In the second model we study the atom-vapor based PNRD from first principles, including quantum mechanical treatment of the electromagnetic field. We analyze a photon detector model that combines coherently controlled absorption of light and resonance fluorescence to achieve photon counting at room temperature. In particular we identify the fundamental limits to this particular scheme of photon detection. We show that there exists a time-energy uncertainty between the incident pulse strength and the time period of the incident pulse. We verify the role of a large ensemble of atoms in boosting the efficiency of such a detector.

Lastly, we show the application of PNRD technique to enhance laser range finding and light detection and ranging. We present a technique that improves the signal-to-noise-ratio (SNR) of range-finding, sensing, and other light-detection applications. The technique filters out low photon numbers using PNRD. This technique has no classical analog and cannot be achieved with classical detectors. We investigate the properties of our technique and show under what conditions the scheme surpasses the classical SNR. Finally, we simulate the operation of a rangefinder, showing improvement with a low number of signal samplings and confirming the theory with a high number of signal samplings.

CHAPTER 1
INTRODUCTION

We are in very exciting times of quantum optics and communication. Sometime ago quantum computers, and quantum networks were just theoretical ideas and their full implementation seemed so distant. However, in recent years there has been an astounding progress in the field. As the Moore's law is beginning to hit the physical limit, the inclusion of quantum effects is indispensable with small scale size of transistors [1, 2]. The launch of the Chinese quantum satellite Micius in 2016, has led to a lot of excitement in both Physics community as well as the general public. A major accomplishment of Micius is long-range secure quantum communication.

Qubits are already being used for creating secret keys, to encode classical information. This technique is known as quantum-key distribution (QKD). The record distance for QKD to date is 400 Km at 6.5 kbit/s, which has been achieved by the group at the university of Geneva, led by Alberto Boaron [3]. In addition to quantum communication, quantum effects can lead to tremendous development in the field of quantum metrology with improved resolution, and sensing. These advances have also lead to physical challenges that need to be tackled, in order to realize the full potential of quantum technologies.

Another important fundamental technology requirement for the success of quantum communications, and network, are reliable single-photon detectors (SPD). The single photon technology connects the classical to the quantum world. Single-photon technology can be used for example in Bell state testing that can answer fundamental questions of non-local realism [4], and generation of verifiable random numbers [5, 6]. Single-photon technologies operate at the fundamental limit of electro-magnetic signal strength, hence find applications in various sensors [7, 8]. There are several applications that rely on the single-photon technology, like quantum cryptography protocols [9, 10, 11], quantum repeaters for use in quantum communication [12, 13], and quantum computation [14]. For example, in boson sampling the effect of SPD is clearly demonstrated [15]. Another example is quantum receivers that are important in all quantum network protocols as

they need to discriminate between non-orthogonal states at error rates below the standard quantum limit (SQL). Reliable SPDs are vital to close the loop-holes that exist in the fundamental tests of quantum mechanics pertaining to non-locality [16].

The desired characteristics of reliable SPDs includes high detection efficiency, low dark counts, fast response time, and low time-jitter. In several applications of quantum computation, and the study of quantum nature of light, photon-number resolving detectors (PNRD) play a vital role. PNRD should be able to unambiguously tell the difference for example, between one, and two photons. Most of the current photon-number-resolving detectors either have low efficiency or are plagued with high dark count rates and low response time. Moreover, they have to be maintained at extremely low temperature to yield high efficiency. For single-shot measurements, high photon-number detection efficiencies is required compared to ensemble based applications. PNRD can also be used to recover photon statistics, given low uncertainty in the positive-operator valued measure (POVM) elements. The applications for PNRD include quantum metrology, quantum imaging, quantum information, and foundations of quantum mechanics. The most popular type of PNRD are the Transition-Edge Sensors (TES), but these require advanced cryogenic equipment, which are not easily accessible [17, 18, 19].

In this thesis, I will present two theoretical models for photon detectors. Both of them are meant to operate at room temperatures. The schemes presented in this thesis will be ideal for applications in a variety of fields that require photon-statistics such as astronomy, microscopy, quantum cryptography, and optical quantum computing such as boson sampling.

In the rest of this introduction, I will give a brief description of the theory necessary to help the reader understand the topics presented. First I will develop some key concepts in quantum optics including coherent light, single-mode squeezing, two-mode squeezing, non-linear process to squeeze light, and the respective photon statistics of light sources mentioned. Then I will talk about two-level atomic system and extend their theory to three-level atoms and discuss their use in the field of quantum technology.

In chapter 2, I will present a theoretical model for photon-number resolving detector at room temperature, using two-mode squeezing device. Next, in chapter 3, another room temperature photon-number resolving detector using an atomic vapor will be presented. In chapter 4, I will present an application of PNRDs in one particular sensing method, namely, laser range finding and light detection and ranging (LIDAR). Increasing the range requires sensitive detectors, and more recently, single-photon detectors (SPDs) [20], and photon-number-resolving detectors (PNRDs) [21, 22] have been used for this purpose. We know that many proven quantum effects are not a result of using quantum states, but of using quantum detection of these states [23]. In this chapter I will discuss how using PNRDs with threshold detection can give quantum advantage, hence signal-to-noise ratio improvement.

1.1 Quantum Optics

In this section starting from the Maxwell's equation, I will discuss the quantization of the field, the quadrature operators to define the field. Then I will review the coherent state of light, and the squeezed light, as well as their photon statistics [24].

The Maxwell's equations to describe the light field in free space are,

$$\begin{aligned} \nabla \times \mathbf{E} &= -\frac{\partial \mathbf{B}}{\partial t}, \\ \nabla \times \mathbf{B} &= \mu_0 \epsilon_0 \frac{\partial \mathbf{E}}{\partial t}, \\ \nabla \cdot \mathbf{B} &= 0, \\ \nabla \cdot \mathbf{E} &= 0, \end{aligned} \tag{1.1}$$

where **E**, and **B** are the electric and magnetic fields respectively. The solution to the Maxwell's

equations satisfying the boundary conditions,

$$E_x(z,t) = \sqrt{\frac{2\omega^2}{V\epsilon_0}} q(t) \sin(kz) \tag{1.2}$$

$$B_y(z,t) = \left(\frac{\mu_0\epsilon_0}{k}\right) \sqrt{\frac{2\omega^2}{V\epsilon_0}} \dot{q(t)} \cos(kz) \tag{1.3}$$

where ω is the frequency of the field, and $k = \omega/c$, $q(t)$ acts like the canonical position, and $p = \dot{q}(t)$ is the canonical momentum. Now, the classical Hamiltonian of this single-mode field is equivalent to that of a simple harmonic oscillator, $H = \frac{1}{2}(p^2 + \omega^2 q^2)$, of unit mass, and the **E**, and **B** fields are the canonical position and momentum. Now, we replace the canonical variables q and p with a pair of non-commuting operators, $\hat{q}$ and $\hat{p}$ such that $[\hat{q}, \hat{p}] = i\hbar\hat{I}$. The Hamiltonian then becomes $\hat{H} = \frac{1}{2}(\hat{p}^2 + \omega^2\hat{q}^2)$. Next, we rewrite $\hat{q}$ and $\hat{p}$ in terms of a pair of non-Hermitian annihilation ($\hat{a}$), and creation ($\hat{a}^\dagger$) operators defined as,

$$\hat{a} = \sqrt{\frac{1}{2\hbar\omega}}(\omega\hat{q} + i\hat{p}) \tag{1.4}$$

$$\hat{a}^\dagger = \sqrt{\frac{1}{2\hbar\omega}}(\omega\hat{q} - i\hat{p}). \tag{1.5}$$

The annihilation and creation operators obey the commutation relation $\left[\hat{a}, \hat{a}^\dagger\right] = 1$. Using these results, we can write the quantized version of the field as

$$\begin{aligned} \hat{E}_x &= \mathcal{E}_0(\hat{a} + \hat{a}^\dagger)\sin(kz), \\ \hat{B}_y &= -i\mathcal{B}_0(\hat{a} - \hat{a}^\dagger)\cos(kz), \end{aligned} \tag{1.6}$$

where $\mathcal{E}_0$, and $\mathcal{B}_0$ represent the electric, and magnetic fields per photon. Also, from Eq. 1.6, we see that $\hat{E}$ and $\hat{B}$ do not commute. Using this new set of operators, the Hamiltonian can now be

written as

$$\hat{H} = \hbar\omega \ \ \hat{a}^\dagger \hat{a} + \frac{1}{2} \ \ . \tag{1.7}$$

The operator $\hat{a}^\dagger \hat{a}$ is defined as the number operator $\hat{n}$, which gives the photon number in the field. Lastly, we introduce the so-called "quadrature" operators $\hat{X}_1$, and $\hat{X}_2$ defined as,

$$\hat{X}_1 = \frac{1}{2}(\hat{a} + \hat{a}^\dagger) \tag{1.8}$$

$$\hat{X}_2 = \frac{1}{2i}(\hat{a} - \hat{a}^\dagger). \tag{1.9}$$

Finally, we are able to write the quantized electromagnetic field in terms of the quadratures in the following way

$$\hat{E}_x = 2\epsilon_0[\hat{X}_1 \cos(\omega t) + \hat{X}_2 \sin(\omega t)) \sin(kz]. \tag{1.10}$$

1.1.1 Coherent state

The radiation emitted by a classically oscillating current distribution is represented by a coherent state $|\alpha\rangle$. It is the state of light field generated by most lasers. The eigenstate of annihilation operator is a coherent state,

$$\hat{a}|\alpha\rangle = \alpha|\alpha\rangle. \tag{1.11}$$

The coherent state representation in the number state bases can be written as

$$|\alpha\rangle = e^{|\alpha|^2/2} \sum_{n=0}^{\infty} \frac{\alpha^n}{\sqrt{n!}} |n\rangle. \tag{1.12}$$

Another way to describe coherent states is that they are the displaced form of harmonic oscillator ground state,

$$\hat{D}_\alpha|0\rangle = |\alpha\rangle, \text{where} \quad \hat{D}_\alpha = e^{\alpha\hat{a}^\dagger - \alpha^*\hat{a}}. \tag{1.13}$$

and $\hat{D}_\alpha$ is the displacement operator, which displaces the vacuum state by an amount α as depicted in Fig. 1.1. Also, the coherent light states are minimum uncertainty states, $\triangle\hat{X}_1\triangle\hat{X}_2 = \frac{1}{4}$.

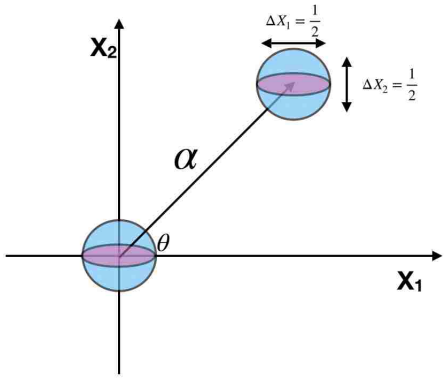

Figure 1.1. Phase-space picture showing the different states of light. The circle at the origin represents quantum vacuum state. The displaced blue circle represents the displaced vacuum state a.k.a coherent light state. The angle θ represents the phase angle of the field. The pink ellipse at the origin is a squeezed vacuum state and the shifted pink ellipse represents the displaced squeezed vacuum, by amount $|\alpha|$.

1.1.2 Squeezed Light

In the previous section we found that the coherent states minimize the uncertainty states and both the quadratures show equal uncertainties $\triangle\hat{X}_1 = \triangle\hat{X}_2 = \frac{1}{2}$. A squeezed state also minimizes the uncertainty product, but the quadratures exhibit unequal quantum fluctuations as shown in Fig. 1.1. In other words, the quantum fluctuations in one quadrature are reduced below their values seen in coherent state ($\triangle\hat{X}_1 < \frac{1}{2}$ or $\triangle\hat{X}_2 < \frac{1}{2}$). Next, I will discuss how squeezed light is generated, and define the unitary squeezing operator. The generation of squeezed light occurs via interaction between light field and medium. The light field interaction with the medium results in non-linear polarization response proportional to $\chi^{(i)}$, ith order susceptibility. The Hamiltonian in the interaction picture can be written as

$$\hat{H}_I = i\hbar(\chi^{(2)}\alpha^*\hat{a}^2 - \chi^{(2)}\alpha\hat{a}^{\dagger 2}),$$
$$\hat{H}_I = i\hbar(\alpha^2\chi^{(3)}\hat{a}^2 - \alpha^2\chi^{(3)}\hat{a}^{\dagger 2}), \tag{1.14}$$

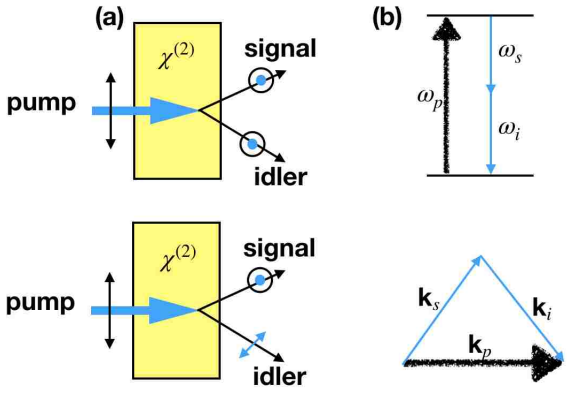

Figure 1.2. The schematic diagram of parametric-down conversion to produce squeezed light. (a) The top figure shows the degenerate-parametric down-conversion where the signal and idler photons are in the same modes. The bottom figure shows the non-degenerate-parametric down conversion, where the signal and idler photons are in different modes. (b) Energy and momentum conservation between the pump (p), signal (s) and idler (i) photons [4].

where, Eqns. 1.14 represent the degenerate parametric amplification process, and degenerate four-wave mixing process respectively. The non-linear medium $\chi^{(2)}, \chi^{(3)}$, interacts with the pump light (pulsed or continuous-wave laser) of frequency ω_p which decays into two photons of equal frequency $\omega_p/2$, as seen in Fig. 1.2(a). The squeeze operator obtained from the interaction Hamiltonian can be defined as

$$\hat{S}(\xi) = \exp\left[\frac{1}{2}(\xi^*\hat{a}^2 - \xi\hat{a}^{\dagger 2})\right], \tag{1.15}$$

where $\xi = re^{i\theta}$, r is the squeezing parameter, and θ is the squeezing angle. The action of squeezing operator on the vacuum gives a squeezed state and the quantum fluctuations in the quadratures for $\theta = 0$ are $\triangle\hat{X}_1^2 = \frac{1}{4}e^{-2r}$, and $\triangle\hat{X}_2^2 = \frac{1}{4}e^{2r}$. So far I have discussed single-mode squeezed light. Now I will briefly introduce the two-mode squeezed light. The states produced by non-degenerate parametric amplification are called two-mode squeezed vacuum states (TMSV) and are entangled. The interaction Hamiltonian is given as,

$$H_I = \imath\hbar\chi^{(3)}(\alpha^*\hat{a}\hat{b} - \alpha\hat{a}^\dagger\hat{b}^\dagger) \tag{1.16}$$

which represents the non-degenerate parametric down-conversion where the pump field (α) is converted into two photons in modes a, and b shown in Fig. 1.2(a). Another way to generate the TMSV is by using the process of four-wave mixing, which is also a $\chi^{(3)}$ process. In this case, instead of three waves, there are four waves. Two pump fields are converted into two correlated fields, signal (s) and idler(i) such that $\omega_{p1} + \omega_{p2} = \omega_s + \omega_i$.

1.2 Quantum Treatment of Atom-Field Interaction

The density matrix of a quantum system can be defined as

$$\hat{\rho} = \sum_{\psi} P_{\psi} |\psi\rangle\langle\psi| \tag{1.17}$$

The Hamiltonian for the atom-field consists of unperturbed $\hat{\mathcal{H}}_0$, and interaction part $\hat{\mathcal{H}}_1 = -e\hat{x}E(t)$,

$$\begin{aligned} \mathcal{H}_0 &= \hbar\omega_a |a\rangle\langle a| + \hbar\omega_b |b\rangle\langle b| \\ \mathcal{H}_1 &= -(\mathcal{P}_{ab}|a\rangle\langle b| + \mathcal{P}_{ba}|b\rangle\langle a|)E(t). \end{aligned} \tag{1.18}$$

where $\mathcal{P}_{ab}, \mathcal{P}_{ba}$ are the matrix elements of the electric dipole moment, and the field of the atom is given by $E(t)$. Also, a and b refer to the two atom levels. We derive the equation of motion for the density matrix elements, and obtain the probability of the atom in levels a, and b using $\hat{\dot{\rho}} = -\frac{i}{\hbar}[\mathcal{H}, \rho]$. Also, we need to include the decay of atomic levels due to spontaneous emission. We can add the phenomenological decay term to the equation of motion for density matrix. The matrix elements of the spontaneous decay, Γ is $\langle n|\Gamma|m\rangle = \gamma_n \delta nm$. Therefore the equation of motion becomes,

$$\hat{\dot{\rho}} = -\frac{i}{\hbar}[\mathcal{H}, \rho] - \frac{1}{2}\{\Gamma, \rho\}. \tag{1.19}$$

We can easily extend this to many level systems, then the *ij*th element of the density matrix is

$$\hat{\dot{\rho}}_{ij} = -\frac{i}{\hbar} \sum_k (\mathcal{H}_{ik}\rho_{kj} - \rho_{ik}\mathcal{H}_{kj}) - \frac{1}{2} \sum_k (\Gamma_{ik}\rho_{kj} + \rho_{ik}\Gamma_{kj}). \tag{1.20}$$

The Hamiltonian for a two-level system can be extended to explain more complicated systems such as a laser, as well as a simplified picture of spontaneous emission [25].

CHAPTER 2
ROOM-TEMPERATURE PHOTON-NUMBER-RESOLVED DETECTION USING A TWO-MODE SQUEEZER

2.1 Introduction

Photon-number-resolving detectors (PNRD) are crucial to the field of quantum optics, and quantum information processing. PNRDs can be useful in two major classes of application: Single-shot measurement of photon-number, and ensemble measurements for photon number statistics. Single-shot photon number measurement is useful in the field of linear optical quantum computing, quantum repeaters, entanglement swapping, and conditional state preparation [26, 27, 28, 29, 30]. Ensemble-measurement based PNRDs can be used in quantum interferometry for measuring photon statistics, characterization of quantum light sources, and improving sensitivity and resolution. [31, 32, 33, 34, 35]. For example, a true single-photon source is important for quantum key distribution. The ultimate security of the key can be compromised if the source emits more than one photon in the same quantum bit state. Hence, a photon-number resolving detector that can characterize the single-photon source accurately is vital for the success of quantum key distribution [36, 37]. Also, the reconstruction of photon-statistics of unknown light sources by ensemble measurements can be used to determine the nature of the light source (classical or non-classical), the and detection of weak thermal light and coherent light. Therefore, a desirable feature of a PNRDs is accurate detection of the number of photons. In this paper, we propose a room-temperature photon-number-resolving detector using a two-mode squeezing device that finds its application in the reconstruction of photon statistics of unknown light states, and characterization of non classical light resources. For example, source characterization for enhanced quantum key distribution, and detection of weak thermal light.

This chapter previously appeared as Elisha S. Matekole, Deepti Vaidyanathan, Kenji W. Arai, Ryan T. Glasser, Hwang Lee, and Jonathan P. Dowling, "Room-temperature photon-number-resolved detection using a two-mode squeezer", Physical Review A 96, 053815, Published 7 November 2017.

Commonly used photon detectors are the bucket or on-off detectors. These detectors can only distinguish between zero or more photons. Photon-detectors typically include avalanche-based photodiodes, such as the visible light photon counters [33, 38], two-dimensional arrays of avalanche photodiodes [39, 40], time-multiplexed detectors [41, 42, 43], photomultipliers [44], and weak avalanche-based PNRD [45]. Most of these detectors have a high dark-count rate at room temperature, and are not sensitive to photon number greater than one. Therefore, they cannot be used in applications that require photon statistics. For example, the time-multiplexed detectors, split the incident pulse of photons into several temporal modes, which can be detected with non-photon-number-resolving detectors. One way to do this is to store the incident light pulse in a fibre loop, an optical switch couples the light pulse to the loop. Another asymmetric coupler allows only one photon per pulse to leave the cavity. Then a SPD is used to detect the output, and reconstruct the number of photons in the pulse [46]. The issue with this technique is the long response time. Also there is an overlap between the residual photons from the previous pulse and the current pulse. This leads to an over estimation of the number of photons. Another type of PNRD is a transition edge sensor (TES), which is a superconducting microbolometer or a superconductor based thermometer. These detectors operate near the superconductor to metal transition temperature, such that during the transition a small change in the temperature there is a big increase in the resistance which can be used to measure the energy. These detectors are highly efficient but they operate at extremely low temperatures and have a slow response time depending on the thermal properties of the material [37, 17, 18, 19].

Another superconductor-based PNRD uses parallel superconducting-nanowires, which can resolve finite number of photons at telecommunication wavelengths [47, 48]. Recently, atomic-vapor-based photon-number-resolving detectors have also been proposed [49]. The merit of any PNRD is determined by detector efficiency, dark count rate, and response time. Most of the current photon-number-resolving detectors either have low efficiency or are plagued with high dark-count rates and low response time. Moreover, they have to be maintained at extremely low temperature

to yield high efficiency.

A two-mode squeezed vacuum (TMSV), also known as the twin-beam state, is an entangled state containing strong correlations between the two beams. However, individually these modes are not squeezed and resemble a thermal state [50, 51, 52]. Here I will discuss the properties of two-mode squeezed vacuum briefly. As discussed in chapter one, the two-mode squeezed vacuum operator is given by

$$\hat{S}_2(\xi) = exp(\xi^* \hat{a}\hat{b} - \xi \hat{a}^\dagger \hat{b}^\dagger). \tag{2.1}$$

Also, the two-mode squeezing operator cannot be written as a product of two single-mode squeezing operators, therefore, the two-mode squeezed light is highly correlated. In other words the quantum noise of the two modes are not individually squeezed, but as a superposition of the two modes. The following representation of the field quadrature further illustrates this,

$$\begin{aligned} \hat{X}_1 &= \frac{1}{2^{3/2}}(\hat{a} + \hat{a}^\dagger + \hat{b} + \hat{b}^\dagger), \\ \hat{X}_2 &= \frac{1}{2^{3/2} i}(\hat{a} - \hat{a}^\dagger + \hat{b} - \hat{b}^\dagger). \end{aligned} \tag{2.2}$$

The field quadratures obey the commutation relation $\left[\hat{X}_1, \hat{X}_2\right] = \frac{i}{2}$. Let us call the two field modes produced by the interaction of the coherent light state with the non-linear medium as *a*, and *b*. The transformation of the field operators by two-mode squeezing field can be derived by using Baker-Hausdorff lemma,

$$\begin{aligned} \hat{S}_2(\xi)^\dagger \hat{a} \hat{S}_2(\xi) &= \hat{a} \cosh r - e^{\imath\theta} \hat{b}^\dagger \sinh r, \\ \hat{S}_2(\xi)^\dagger \hat{b} \hat{S}_2(\xi) &= \hat{b} \cosh r - e^{\imath\theta} \hat{a}^\dagger \sinh r. \end{aligned} \tag{2.3}$$

Here the squeezing angle is represented by θ. When $\theta = 0$, the fluctuations in the two-mode squeezed quadratures are $\langle \Delta \hat{X}_1 \rangle^2 = \frac{1}{4} e^{-2r}$, and $\langle \Delta \hat{X}_2 \rangle^2 = \frac{1}{4} e^{2r}$. It is interesting that this is the same expression as that of single-mode squeezed light. The Fock state representation of the TMSV

is given as

$$|\xi\rangle_2 = \frac{1}{\cosh r} \sum_{n=0}^{\infty} (-1)^n e^{in\theta} (\tanh r)^n |n, n\rangle. \tag{2.4}$$

Readers interested in detailed derivations of this state are advised to refer to ref. [24]. The average number of photons in each of the two modes is $\hat{n}_a = \hat{n}_b = \sinh^2 r$, and both the modes follow super-poisson statistics. When we trace over one of the two modes, the field in the other mode is a thermally distributed state with average photon number of $\sinh^2 r$. As mentioned earlier their exists extremely strong correlations in the two modes. Therefore the intensity difference of these twin-modes is zero, and the variance of the intensity difference is also zero.

$$\langle \Delta(\hat{n}_a - \hat{n}_b)^2 \rangle = \Delta(\hat{n}_a)^2 + \Delta(\hat{n}_b)^2 - 2\,\mathrm{cov}(\hat{n}_a, \hat{n}_b), \tag{2.5}$$

where the covariance is calculated to be $\frac{1}{4}\sinh^2 2r$. This indicates the presence of strong intermode correlations. When the covariance of two light modes is zero, it implies that there is no correlation between the modes. Due to the correlations and symmetry between the two modes, the average photon number in each mode is the same. Also, the covariance between the two modes describe the inter-mode correlations. TMSV is produced experimentally via non degenerate parametric downconversion or four-wave mixing [24, 53]. Recently TMSV light has proven to be extremely useful in quantum metrology [54, 55] and quantum information processing [56].

2.2 Photon-Number Resolving Scheme

The setup used for the proposed scheme is shown in Fig. 2.1. An unknown N-photon state is incident on one port of the FWM and a coherent-light state with average photon number $\bar{n}_\alpha$ is incident on the second port. The average intensity-intensity correlations $\langle \hat{C} \rangle$ and the noise in the intensity-intensity correlations $\Delta\hat{C}$ are measured at the output to detect the input photon number.

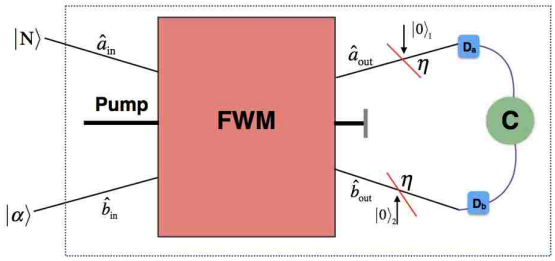

Figure 2.1. The schematic diagram of a room-temperature number-resolving photon detector. The two-mode inputs to the four-wave mixer (FWM) are N-photon Fock states, and a coherent state of light $|\alpha\rangle$, $\hat{a}_{\rm in}(\hat{a}_{\rm out})$ and $\hat{b}_{\rm in}(\hat{b}_{\rm out})$ represent the mode operators of input (output) light beams. The average intensity-intensity correlations and the noise in the intensity-intensity correlations are detected at the output. The losses due to imperfect squeezing and the inefficiency of the photon detectors, are modeled by adding fictitious beam splitters each of overall transmissivity η, where the vacuum modes are denoted by $|0\rangle_1$ and $|0\rangle_2$.

The operators $\hat{a}$ and $\hat{b}$ after interacting with the two-mode squeezer become

$$\begin{aligned} \hat{a} &\rightarrow \hat{a}\mu - \hat{b}^{\dagger}, \nu \\ \hat{b} &\rightarrow \hat{b}\mu - \hat{a}^{\dagger}\nu, \end{aligned} \tag{2.6}$$

where $\mu = \cosh(r)$, and $\nu = \sinh(r)$. Intensities $\langle \hat{N}_a \rangle$ and $\langle \hat{N}_b \rangle$ and the intensity difference $\langle \hat{M}_{-}^{ab} \rangle$ at the two output modes are

$$\begin{aligned} \langle \hat{N}_a \rangle &= \bar{n}_s(\bar{n}_\alpha + N) + N + \bar{n}_s, \\ \langle \hat{N}_b \rangle &= \bar{n}_s(\bar{n}_\alpha + N) + \bar{n}_\alpha + \bar{n}_s, \\ \langle \hat{M}_{-}^{ab} \rangle &= N - \bar{n}_\alpha, \end{aligned} \tag{2.7}$$

where $\bar{n}_s$ is the average number of photons in a single-mode squeezed vacuum and is fixed at the value of two in this calculation, corresponding to 10 dB of squeezing [57, 58].

The above equations show that correlations and symmetry between the two modes has been disturbed because of different input modes. In particular $\langle \hat{M}_{-}^{ab} \rangle$ is identically zero for pure TMSV. We exploit this change in the correlations between the two beams to resolve the number of photons

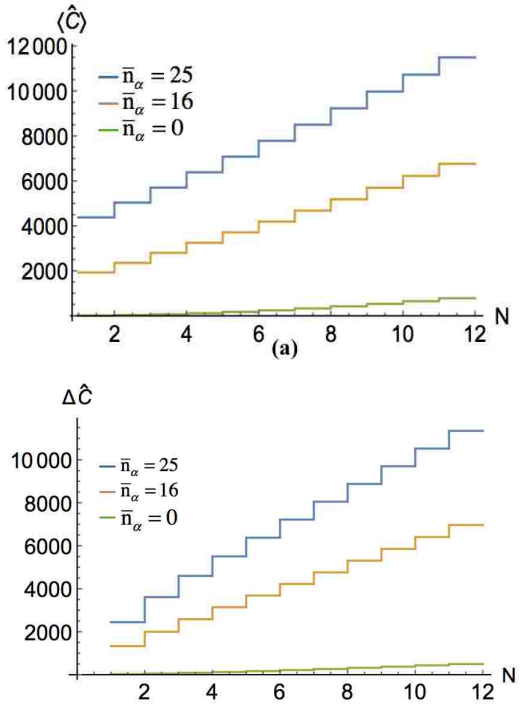

Figure 2.2. (a) and (b) show the average intensity-intensity correlations $\langle \hat{C} \rangle$ and the noise ΔC in the intensity-intensity correlations as a function of input photon number N incident on one port of a two-mode squeezing device with $\bar{n}_s = 2$ respectively: Both $\langle \hat{C} \rangle$ and ΔC increase in steps as the input photon number changes in increments of one. When a single photon is incident, there is huge jump in $\langle \hat{C} \rangle$ and ΔC. $\langle \hat{C} \rangle$ and ΔC for vacuum as input in the second mode shows smaller step sizes than those with coherent-light inputs. Hence the coherent-light state provides a *boost* to the $\langle \hat{C} \rangle$ and ΔC signals. Also this shows that even in the presence of coherent state amplitude fluctuation, we still see the steps in the signal and the noise. Therefore, for a slowly fluctuating coherent state, we expect to observe slowly fluctuating signal while still maintaining the steps, representing the input photon number.

in the input by detecting the average intensity-intensity correlations at the output. The average intensity-intensity correlations signal is calculated from

$$\langle \hat{C} \rangle = \langle N|_a \langle \alpha|_b \hat{N}_a \hat{N}_b |\alpha\rangle_b |N\rangle_a, \tag{2.8}$$

and is given by

$$\begin{aligned}\langle \hat{C} \rangle = &\left(\alpha^2 + 1\right)(N+1)\sinh^4(r) \\ &+ \alpha^2 N(1+\sinh^2(r))^2 \\ &+ \left(\alpha^4 + \alpha^2(2N+3) + (N+1)^2\right)\sinh^2(r) \\ &(1+\sinh^2(r)).\end{aligned} \tag{2.9}$$

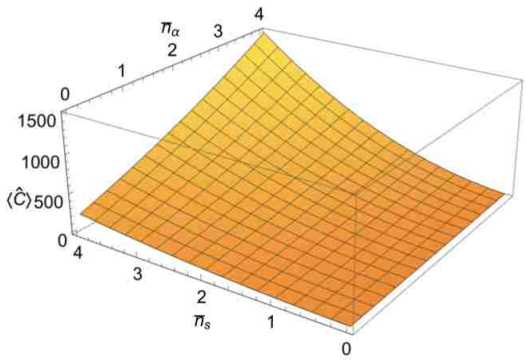

Figure 2.3. The average intensity-intensity correlations signal as a function of $\bar{n}_\alpha$, and $\bar{n}_s$. The signal attains the maximum value at $\bar{n}_\alpha = \bar{n}_s$.

The average intensity-intensity correlations and the standard deviation (noise) of the average intensity-intensity correlations as a function of the input photon state are plotted in Fig. 2.2, (see appendix for the expression of ΔC). From the figure we can see that there is a huge jump in both $\langle \hat{C} \rangle$ and ΔC even when a single photon is incident on the FWM. What is interesting is the amplification of the noise in the intensity-intensity correlations when a single photon is detected. Hence, a large change in ΔC is an indicator of the presence of photon.

In Fig. 2.2, we compare the amplitude of the signal for vacuum and coherent-light input respectively. The steps for the case of nonzero coherent-light input are greatly amplified compared to the vacuum, and hence this provides a boost to the intensity-intensity correlations signal. Thus the purpose of having coherent light as input to the second mode is to amplify the output signal, while

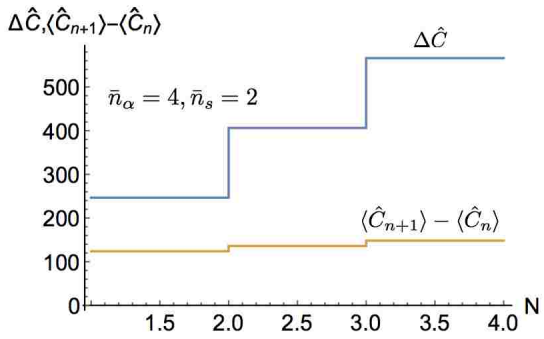

Figure 2.4. Plot comparing the step-size of the average intensity-intensity correlations signal, with the noise.

still displaying the steps as the photon number changes. Our scheme does not require a very strong coherent light source, therefore the possibility of the coherent-light producing its own twin-beam state is ruled out. In order to have a well calibrated nonlinear gain, a feedback system to control the output measured coherent-state amplitude can be used. This will be equivalent to controlling the gain, while showing the jumps in the $\langle\hat{C}\rangle$ or ΔC signals. Both $\langle\hat{C}\rangle$ and ΔC display steps as the number of input photon is increased in steps of one. Therefore, it is possible to know the input photon number by counting the height of steps in $\langle\hat{C}\rangle$ or ΔC. In Fig. 2.3 we show that the $\langle\hat{C}\rangle$ signal is maximum when both $\bar{n}_\alpha$, and $\bar{n}_s$ are equal. Also, both the $\langle\hat{C}\rangle$, and ΔC are comparable in magnitude for any choice of $\bar{n}_\alpha$, and $\bar{n}_s$. Therefore, the step size of $\langle\hat{C}\rangle$ signal can never exceed the noise, ΔC. Hence, the current set-up is not suitable for single shot experiment. In Fig. 2.4 we compare the noise, and the step-size. We can also use the covariance or the correlation in photon number fluctuations as a function of input photon number, shown in Fig. 2.5 as the signal. We

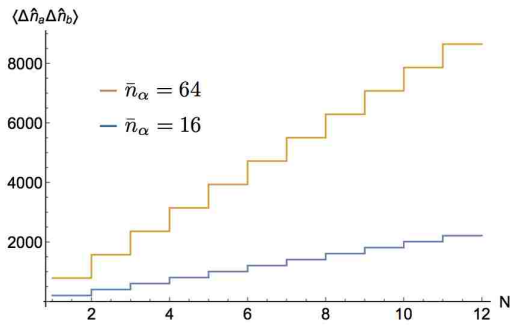

Figure 2.5. Correlation in photon number fluctuations as function of input photon number.

also calculate the two-mode second-order intensity correlation function $g_{12}^{(2)}(0)$ which is defined as $\langle\hat{C}\rangle/(\langle\hat{N}_a\rangle\langle\hat{N}_b\rangle)$ [59], and is calculated at zero time delay. This is another way of describing the

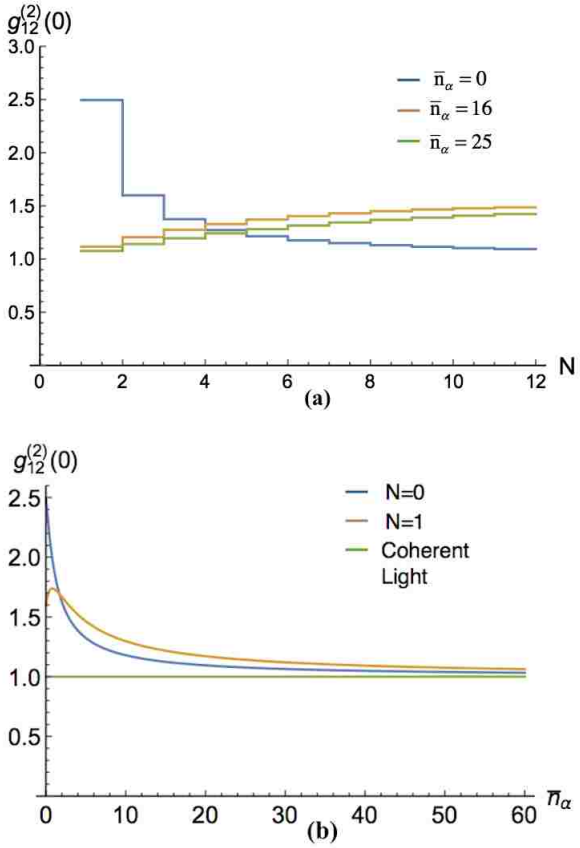

Figure 2.6. (a) Two-mode second-order intensity correlation function $g_{12}^{(2)}(0)$ as a function of number of input photons N for different $\bar{n}_\alpha$, and $\bar{n}_s = 2$. When $\bar{n}_\alpha = 0$, then $g_{12}^{(2)}(0)$ has maximum correlation for N=0. As N increases, $g_{12}^{(2)}(0)$ decreases. When $\bar{n}_\alpha \neq 0$, the correlations increase with N, but still less than that of TMSV. (b) $g_{12}^{(2)}(0)$ as a function of coherent-light amplitude. As the strength of the coherent light is increased the curves for $N = 0$, and $N = 1$ approach the single-mode second-order intensity correlation function $g_1^{(2)}(0)$ for a coherent state asymptotically.

intermode correlations as well as photon bunching. We know that if $g_{12}^{(2)}(0) > 1$, then the light has bunching or represents super-Poisson state. For a two-mode squeezed vacuum light, $g_{12}^{(2)}(0) = 2 + 1/\bar{n}_s$, where $\bar{n}_s$ is the average photon number in a single-mode squeezed vacuum state. The

$g_{12}^{(2)}(0)$ for $|N\rangle_a \otimes |\alpha\rangle_b$ input is

$$g_{12}^{(2)}(0) = \frac{N\bar{n}_\alpha(\bar{n}_s^2 + (1+\bar{n}_s)^2) + ((N+1)^2 + (2N+3)\bar{n}_\alpha + \bar{n}_\alpha^2)\bar{n}_s(1+\bar{n}_s) + (1+N+\bar{n}_\alpha)\bar{n}_s^2}{(\bar{n}_\alpha(1+\bar{n}_s) + (N+1)\bar{n}_s)(N(1+\bar{n}_s) + (1+\bar{n}_\alpha)\bar{n}_s)}. \tag{2.10}$$

In Fig. 2.6.a we plot $g_{12}^{(2)}(0)$ as a function of the coherent-state mean photon number $\bar{n}_\alpha$. As the strength of input coherent light increases, the correlations between the two modes decreases and $g_{12}^{(2)}(0)$ approaches the single-mode second-order intensity correlation function $g^{(2)}(0))$ of a coherent-light state, asymptotically. Also, we see that the presence of a single photon in the input mode is sufficient to reduce the correlations between the two beams.

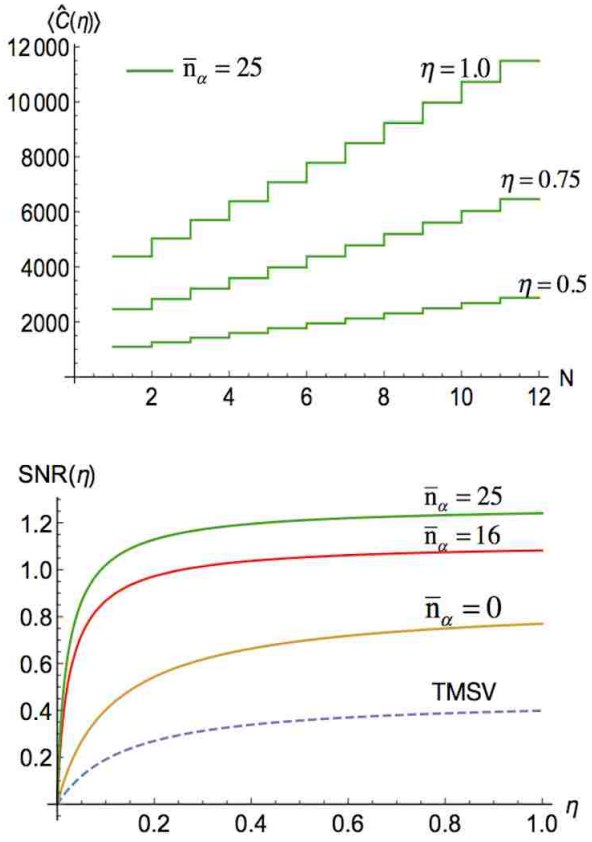

Figure 2.7. (a) Average intensity-intensity correlations signal as a function of input photon number, for different efficiencies represented by η and fixed $\bar{n}_\alpha = 25$. The imperfect two-mode squeezing and correlator can be modeled by adding fictitious beam splitters of transmissivity defined as $\eta = \epsilon T$. Where ϵ represents imperfect squeezing and T represents the efficiency for the photon detector. (b) Signal-to-noise ratio (SNR) as a function of η.

2.3 Effect of Loss

Next, we address the issue of imperfect squeezing and inefficient detection of photons. Generally, the devices used to produce two-mode squeezed light do not perform perfect squeezing and the TMSV is a mixed state. Also, the photon detectors used to detect the photons also have a limited efficiency leading to losses. We model these losses by introducing fictitious beam splitters of transmissivity $\eta = \epsilon T$, where ϵ represents imperfect squeezing and T represents the efficiency of the photon detectors. Therefore the total loss is $1 - \eta$.

Fig. 2.7.a shows $\langle \hat{C} \rangle$ in the presence of losses as a function of the input photon number N. We can see that as the efficiency increases the amplitude of the signal $\langle \hat{C} \rangle$ increases. Also it is possible to attain the same amplitude of the intensity-intensity correlation signal even when the efficiency is low ($\eta \sim 0.5$), by using a stronger coherent-light source to compensate. Hence, the use of coherent light acts as a boost that overcomes the effect of inefficiency in the squeezing and photon detection. Also, unbalanced detector inefficiencies and losses ($\eta_1 = \eta_2$) frequently give rise to adverse effects in experimental quantum optics schemes. However, in our scheme, having detectors of different efficiencies does not degrade the signal, nor the performance, of the PNRD. In Fig. 2.8 we plot the signal-to-noise ratio as a function of η_1 and η_2 and the average intensity-intensity correlations when the two detector efficiencies are different.

Additionally, phase-sensitive detection and amplification schemes are difficult to implement experimentally, as care must be taken to control the (typically) optical phases of the involved beams. Our scheme avoids such difficulties, as the relative phases of the involved modes is not an issue due to the orthogonality of the Fock states. This is true for the thermal state as well, so we can use our scheme to detect weak thermal light. However, it is worth noting that this does not overrule the mode-matching with respect to to the wave-vectors between the different input modes to complete the non-linear process. The signal-to-noise ratio (SNR) is a measure of the system

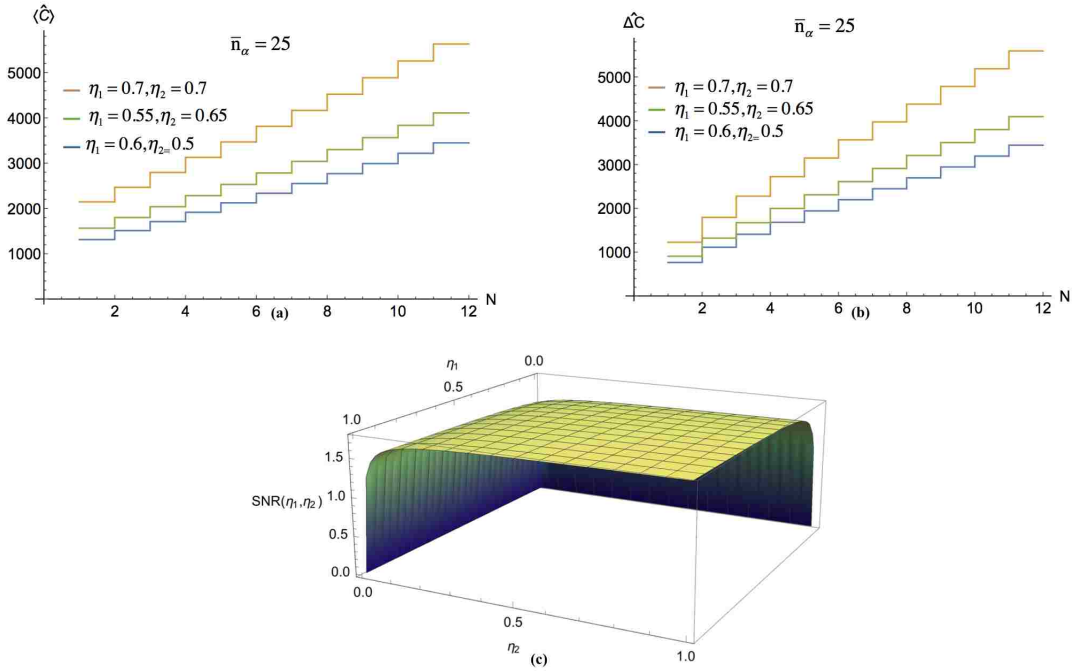

Figure 2.8. (a) and (b) $\langle \hat{C} \rangle$ and $\Delta \hat{C}$ as a function of η_1, and η_2, plotted against the number of input photons for $\bar{n}_\alpha = 25$. (c) SNR plotted against η_1, and η_2.

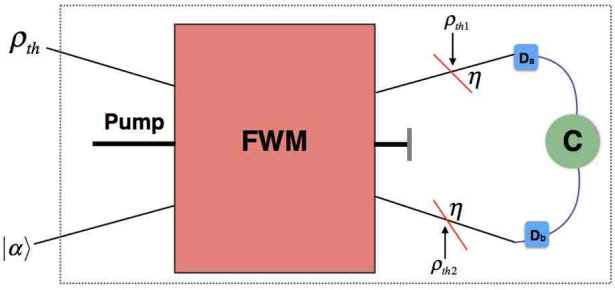

Figure 2.9. The effect of dark counts on the room-temperature number-resolving photon detector. The input number state is approximated with thermal state. The losses due to imperfect squeezing and the dark counts at the output, are modeled by adding fictitious beam splitters each of overall transmissivity η, where the thermal modes are denoted by $\rho_{\rm th1}$ and $\rho_{\rm th2}$.

performance. It is defined as,

$$\mathrm{SNR} = \langle \hat{C} \rangle / \Delta C. \tag{2.11}$$

In Fig. 2.7.b we plot the signal-to-noise ratio as a function of the transmissivity (see appendix for the expression of SNR). The SNR decreases as the transmissivity decreases, however this can be compensated for by increasing the strength of the coherent-light state. We also address the ef-

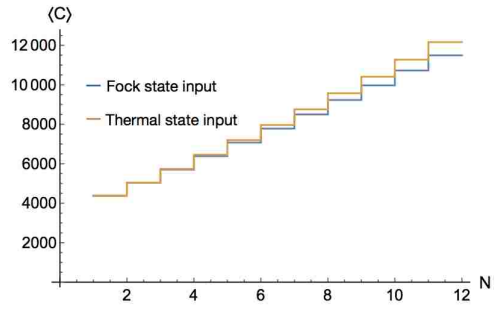

Figure 2.10. Plot comparing the average intensity-intensity correlations as a function of number of input photons *N* for a Fock state input, and a thermal state input. For a thermal input state, *N* is actually $\overline{N}_{\mathrm{thermal}}$, which we have chosen to be an integer increasing in increments of one. This helps in making an easier comparison between the two input states. The average number of photons in the coherent state is $\bar{n}_\alpha = 25$. From the plot we can see that $\langle \hat{C} \rangle$ does not vary much for the two different input states. Hence, we can conclude that the thermal state is a good approximation for input Fock state in the calculation for dark counts.

fect of stray thermal photons on our detection scheme. The thermal photons at room temperature are completely uncorrelated between detectors, and the average number of photons at optical frequencies is very small ($\sim 10^{-40}$) [24]. Again the average number of stray thermal photons at room temperature is of the order of 10^{-3}, which does not effect the detector efficiency.

We mix the stray thermal photons with the output at the two beam splitters as shown in Fig. 2.9. In order to make the dark count calculation easier, we approximate the Fock states with a thermal state enabling us to use Wigner functions [60]. We compare the average intensity-intensity correlations between the input Fock state and the thermal state input in Fig. 2.10. We find that the the two signals do not differ much, hence the the thermal state is a good approximation for the Fock

state as input, and we expect the effect of dark counts on an actual number state $|N\rangle$ to be similar. In Fig. 2.11 we show the effect of stray thermal photons on the intensity-intensity correlations signal and the signal-to-noise ratio. The average number of thermal photons $\overline{N}_{\rm Dark}$ at the room temperature i.e. 300K, have been calculated at the wavelength of 9.7μm.

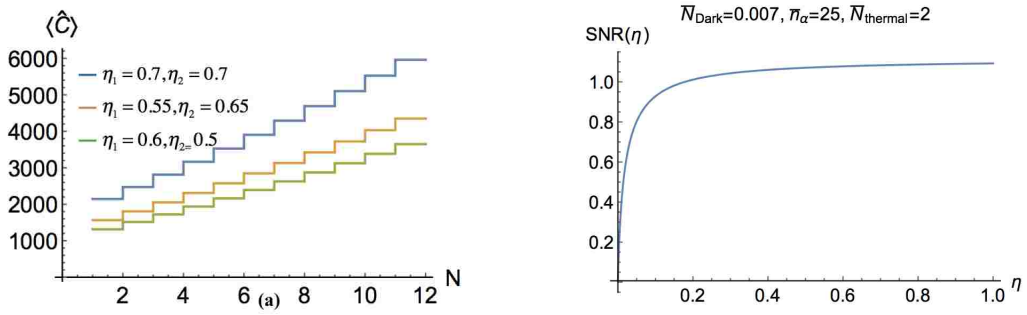

Figure 2.11. (a) Average intensity-intensity correlations signal as a function of input photon number, for different efficiencies represented by η and fixed $\bar{n}_\alpha = 25$. Again, the N used in this plot is the $\overline{N}_{\rm thermal}$. (b) Signal-to-noise ratio in the presence of dark counts against detector efficiency.

2.4 Conclusion

In summary we propose a room-temperature photon-number-resolving detector using a two-mode squeezer. The N-photon number state is fed into a two-mode squeezing device, along with a coherent-light input which amplifies the output signal. The output intensity-intensity correlations signal reports jumps with the changing photon number. Even in the presence of losses, the output signal is strong due to the amplification provided by the coherent light. Hence, we have a high efficiency photon-number-resolving detector. Since the scheme is robust against low detector efficiency, the intensity-intensity correlation measurement can be carried out at room temperature for optical photons.

Additionally since the photon-number states to be counted are boosted (amplified) in the squeezer, dark counts will have negligible effect, particularly at room temperature. Also, this particular setup is robust against any phase fluctuations due to the presence of Fock states which are insensitive to phase. Hence, phase matching is not required, making our technique easier to implement in the lab. Also, the synchronization of the different light pulses will depend mainly on the coherent state.

Most experiments use a continuous-wave coherent light which will give a steady background signal, and is easy to synchronize due to a narrower line width. Moreover, if the temporal profile of the input Fock state is known, it is easy to produce coherent light with the same temporal profile. Also our scheme is robust against coherent state amplitude fluctuation, as we still see the steps in the signal and the noise. Therefore, for a slowly fluctuating coherent state, we expect to observe slowly fluctuating signal but still maintaining the steps, representing the input photon number. Since, both $\langle\hat{C}\rangle$, and ΔC are comparable in magnitude, the step-size never exceeds the noise, ΔC. Therefore, the current set-up is not suitable for a single-shot experiment. Our results can be applied to a wide range of squeezers and each would need to be addressed separately in any experiment. Similarly, the time required for ensemble measurements would depend on the different experiments.

Our scheme is not a general photon-number-resolving detector because it does not implement the POVM $|N\rangle\langle N|$ in the $|N\rangle$ basis. Therefore for thermal light, squeezed light, and coherent light, it will give a distribution around the mean. However, for many applications in quantum technology such as quantum key distribution [61], the photon state is known to be in a Fock state, which is unknown. For such applications our scheme will be ideal. Nevertheless, because of the coherent light boosting, this device should be useful for detecting weak thermal light, squeezed light, and coherent light states that has application for example in quantum LIDAR [23]. In future work, we plan to explore our setup for a multi-frequency mode.

CHAPTER 3
LIMITS TO ATOM-VAPOR BASED PHOTON- NUMBER-RESOLVING DETECTORS

3.1 Introduction

The state-of-the-art photon-detectors mentioned in chapter two rely on getting a detectable signal by converting incident photons to photoelectrons. An alternative approach to resolve photon numbers at room-temperature was proposed by James and Kwiat [62]. This scheme is based on coherently controlled absorption of light and projective quantum-state measurements. The incident single photon is converted to many photons by resonance fluorescence. Around the same time, another proposal to count photons was proposed by Imamoglu in [63], which combines the techniques of ion-trap quantum-state measurements [64] and electromagnetically induced transparency (EIT) [65, 66]. Following along the same lines, Clausen *et al*. proposed a scheme to detect photons based on EIT and resonance fluorescence [67]. However, in the case of trapped ions, typically the system needs to be laser cooled by applying two counter-propagating light beams along the cavity axis. This step is necessary to prepare the system for optical pumping. Also, once the first cycle of detection is completed, a laser re-pumper is required to cool the system for the next detection cycle.

In this paper we revisit the atom-vapor based photon detectors at room-temperature as proposed in reference [62]. A three-level Λ scheme is considered. The detector is prepared using optical pumping to transfer all the atoms in the ground state. The atomic population transfer is achieved by using Stimulated Raman Adiabatic Passage (STIRAP), and the number of photons are detected using a read-out laser, which induces fluorescence.

This chapter previously appeared as Elisha S. Matekole, Hwang Lee, Jonathan P. Dowling, "Limits to Atom Vapor Based Room-Temperature Photon Number Resolving Detection", Phys. Rev. A 98, 033829, Published 28 September 2018.

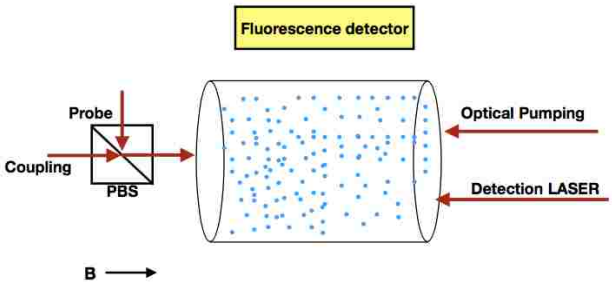

Figure 3.1. Schematic diagram of an atom-based photon detector for ^{133}Cs atom. The polarizing beam splitter (PBS) determines the polarizations of the optical field. The applied magnetic field direction defines the quantization axis.

3.2 Experimental Set-Up

The schematic diagram of the proposed photon detector is shown in Fig. 3.1. We consider an atomic vapor of ^{133}Cs, whose hyperfine structure is shown in Fig. 3.2a.

The radiation to be detected is incident on the cell containing the atoms in the vapor along with a coupling laser. The photons in the incident radiation excite the atoms to a metastable state $|2\rangle$ as shown in Fig. 3.2b. Collisions between atoms, and atom-wall collisions can degrade the atom coherence time. Coating the walls of the vapor cell by paraffin coating reduces the effect of atom-wall collisions [68, 69]. Filling the vapor cell with inert buffer gas reduces the atomic mean free path, hence reduces the probability of wall collisions as well as Cs-Cs collisions [70]. If the number of atoms is large enough, the probability that each photon is absorbed by one atom is close to unity. This allows for the use of lower control laser power in the current scheme. Next the atoms in the metastable state are excited using a readout laser that couples only level $|2\rangle$ $F = 4$, and level $|4\rangle$ $F = 5$ as shown in Fig. 3.2. This implies that only the photons generated by the $|2\rangle - |4\rangle$ transition are counted using photon detection imaging. Hence, resolving the original number of incident photons, by counting the number of fluorescing atoms.

3.3 Optical Pumping

Optical pumping is required for the initialization of the photon detector by transferring all atomic population from $|2\rangle$ into the ground state $|1\rangle$ as shown in Fig. 3.3a. Initially we assume that, both levels $|1\rangle$, and $|2\rangle$ have equal atomic population. Complete optical pumping is important

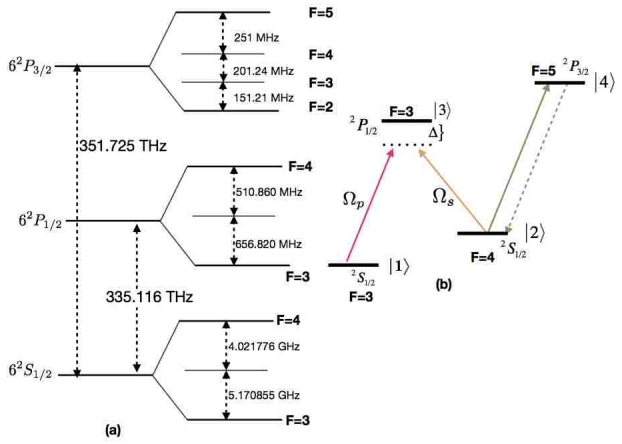

Figure 3.2. (a) Energy level diagram of ^{133}Cs showing the hyperfine structure and the D_1, and D_2 transition [71]. (b) The three level lambda (Λ) system showing the relevant energy levels for the detector. First an ensemble of atoms is prepared in level $|1\rangle$ via optical pumping. Then the atoms in level $|1\rangle$ are excited to level $|2\rangle$ by absorption of photons in the probe field with the help of coupling laser between levels $|1\rangle$ and $|3\rangle$. Finally the atoms in level $|2\rangle$ are detected via fluorescence between levels $|2\rangle$ and $|4\rangle$.

as any atoms not transferred from $|2\rangle$ to $|1\rangle$ would lead to spurious detection at the fluorescence stage. The interaction Hamiltonian of a single three-level atom for the optical pumping technique is given as,

$$\hat{H}_{int} = \frac{\hbar}{2}[\Omega e^{i\Delta t}|3\rangle\langle 2| + |2\rangle\langle 3|\Omega e^{-i\Delta t}] \tag{3.1}$$

where levels $|2\rangle$ and $|3\rangle$ are coupled by a classical laser with Rabi frequency Ω, and Δ represents detuning. We obtain the equations of motion in the rotating-wave frame, using the master equation,

$$\dot{\rho_{22}} = \frac{\Omega}{2i}(\rho_{23} - \rho_{23}^*) + \Gamma_{32}\rho_{33}, \tag{3.2}$$

$$\dot{\rho_{33}} = -\frac{\Omega}{2i}(\rho_{23} - \rho_{23}^*) - 2\Gamma_{32}\rho_{33}, \tag{3.3}$$

$$\dot{\rho_{23}} = -\gamma_{32}\rho_{23} + \frac{i\Omega}{2}(\rho_{33} - \rho_{22}), \tag{3.4}$$

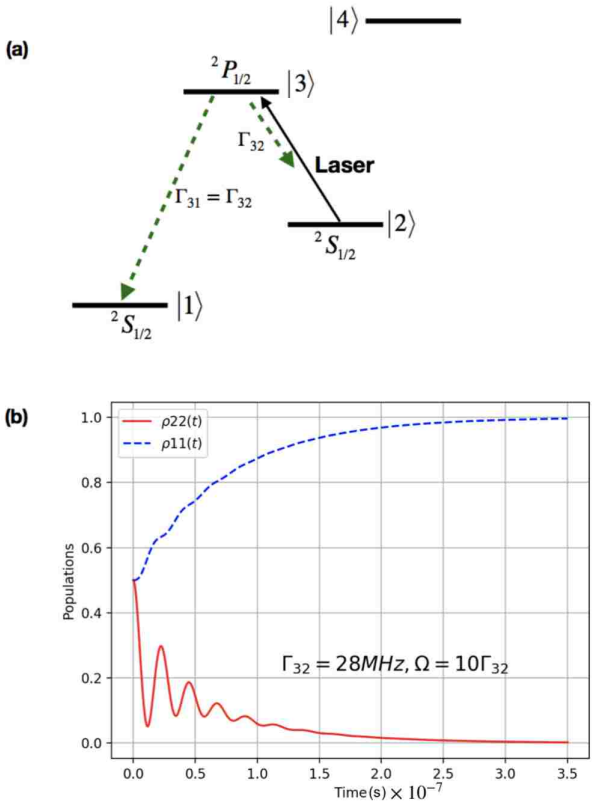

Figure 3.3. (a) Initialization of the photon-number detector by pumping all the atomic population from level $|2\rangle$ to level $|1\rangle$. Levels $|2\rangle$ and $|3\rangle$ are coupled by a classical laser. The atoms from level $|2\rangle$ get transferred to level $|1\rangle$ via level $|3\rangle$. (b) Population evolution of levels $|1\rangle$ and $|2\rangle$ as a function of time for a three-level ^{133}Cs atom. Initially both levels $|1\rangle$ and $|2\rangle$ contain equal number of atoms. When the laser field is applied between levels $|3\rangle$ and $|2\rangle$, atoms from $|2\rangle$ get excited to $|3\rangle$ and spontaneously decay to level $|1\rangle$, with a decay rate Γ_{32}. We have considered zero detuning.

where ρ_{ij} are the matrix elements of the density operator, Γ_{ij} is the spontaneous decay rate from level $|i\rangle$ to $|j\rangle$, and γ_{ij} represents the coherence decay rates. Also, we have assumed the detuning $\Delta = 0$. We plot the time evolution of the population in levels $|1\rangle$, and $|2\rangle$ in Fig. 3.3b. The time taken for all the population to be transferred in $|1\rangle$ is of the order of $0.35\mu s$. Once all the the atoms are pumped to level $|1\rangle$, we are ready for the next step of detecting photons.

3.4 STIRAP

3.4.1 Classical STIRAP

Stimulated Raman Adiabatic Passage (STIRAP) was originally used in population transfer between rotational or vibrational energy levels, to study the dynamics of small molecules [72]. Peter Zoller used STIRAP to manipulate population distribution over quantum states, sparking an interest in the quantum optics community to investigate STIRAP in detail [73]. In quantum optics STIRAP is used in the creation of general quantum state manipulation. In quantum information, STIRAP can employed in the construction of qubit states by controlled superposition of two states with high fidelity [74, 75, 76]. STIRAP is a process that involves a near perfect transfer of population from one state to another via an intermediate state. The key terms that define STIRAP are coherent, two pulses coupling a three level atomic system, with an adiabatic interaction. The success of STIRAP depends on coherent radiation fields. The time required for the coherent pulses to induce population transfer should be shorter than coherence time. It is the time-period during which the effects of decoherence induced by the environment can be neglected. The Rabi frequency is proportional to the coupling strength of the two levels. There are two kinds of detuning in the three-level system i.e. one-photon detuning Δ, and two-photon detuning δ. Again, detuning is the mismatch in the energy difference between the Bohr transition frequencies of the two levels and the incident field. The second step of the atom-based photo-detection is STIRAP, which is used to transfer population between two atomic levels via an intermediate state [77]. Here we consider a two-photon Raman excitation to level $|2\rangle$. The probe field (containing the photons to be detected) along with a strong coupling laser field is introduced in the cell containing the atoms. The interaction Hamiltonian for a single three-level atom describing the STIRAP process is,

$$\hat{H}_{int} = \frac{\hbar}{2}[\Omega_p(t)\hat{\sigma}_{31}e^{i\Delta t} + \Omega_s(t)\hat{\sigma}_{32}e^{i\Delta t} + \text{h.c}], \tag{3.5}$$

$\hat{\sigma}_{ij} = |i\rangle\langle j|$ is the atomic projection operator (i,j=1,2,3). Ω_p and Ω_s represents the Rabi frequency of the photon and coupling lasers respectively, Δ represents the detuning of the lasers from the transition frequencies ω_{31} and ω_{32}.

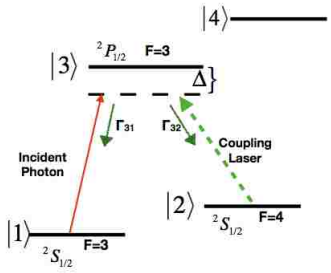

Figure 3.4. The photons in the incident pulse are absorbed by atoms in level $|1\rangle$, which are excited to level $|2\rangle$ with the assistance of coupling laser. Γ_{31} and Γ_{32} are the spontaneous decay rates from level $|3\rangle$ to levels $|1\rangle$ and $|2\rangle$ respectively. The detuning between $|3\rangle$ and the incident fields is given by Δ.

We consider the well-known counter-intuitive pulse sequence in this analysis. First the Stokes pulse is on, such that all the population is in level $|1\rangle$ at some initial time (t_i). Then the probe pulse is on, driving the transition from level $|1\rangle$ to $|2\rangle$ via $|3\rangle$ at final time (t_f). The time-dependence of the Rabi frequency is controlled by suitably delayed laser pulses given as

$$\Omega_s(t) = \Omega_s(0)e^{-\frac{(t+\tau)^2}{2T^2}},$$
$$\Omega_p(t) = \Omega_p(0)e^{-\frac{(t-\tau)^2}{2T^2}}, \tag{3.6}$$

where $\Omega_p(0)$, and $\Omega_s(0)$ represent the maximum amplitude of the Rabi frequency of the probe and coupling lasers. *T* represents the time duration of the two pulses, and τ represents the time delay. The pulse sequence is extremely important in the success of STIRAP. A counterintuitive pulse sequence is not sensitive when $\Delta = 0$. When the pulse sequence is intuitive i.e. the probe pulse precedes the Stokes pulse, there first exist Rabi oscillations between levels $|1\rangle$ and $|3\rangle$, followed by Rabi oscillations between $|2\rangle$ and $|3\rangle$ when S-pulse is on. Now this ordering of pulses is sensitive to detuning. In addition to this, if the two pulses overlap, there exists, Rabi oscillations

independent of Δ, and the population evolution from 0 to 1, depending on detuning and the pulse area. However, a counter-intuitive pulse sequence is robust against pulse area, the value of Δ, pulse shape etc.,this makes STIRAP a robust technique, which is desirable especially in quantum information processing. Using the master equation, we obtain the following equations of motion for the given interaction Hamiltonian;

$$\begin{aligned}
\dot{\rho}_{11}(t) &= \frac{i\Omega_p(t)}{2}(\rho^*_{13}(t) - \rho_{13}(t)) + \Gamma_{31}\rho_{33}(t), \\
\dot{\rho}_{13}(t) &= (i\Delta - \frac{\gamma_{31}}{2})\rho_{13}(t) + \frac{i}{2}\Omega_p(t)(\rho_{33}(t) - \rho_{11}(t)), \\
&\quad - \frac{i}{2}\Omega_s(t)\rho_{12}(t), \\
\dot{\rho}_{22}(t) &= -\frac{i\Omega_s(t)}{2}(\rho_{32}(t) - \rho^*_{32}(t)) + \Gamma_{32}\rho_{33}, \\
\dot{\rho}_{32}(t) &= -(i\Delta + \frac{\gamma_{32}}{2})\rho_{32}(t) - \frac{i}{2}\Omega_s(t)(\rho_{33}(t) - \rho_{22}(t)), \\
&\quad + \frac{i}{2}\Omega_p(t)\rho_{12}(t), \\
\dot{\rho}_{12}(t) &= \frac{i}{2}\Omega_p(t)\rho_{32}(t) - \frac{i}{2}\Omega_s(t)\rho_{13}(t) - \frac{\gamma_{21}}{2}\rho_{12}(t),
\end{aligned} \tag{3.7}$$

where $\Gamma_{31(32)}$ are the spontaneous emission rates out of state $|3\rangle$ to level $|1\rangle(|2\rangle)$. The coherence decay rates are given by γ_{31}, γ_{32}, and γ_{21} [78]. The Doppler shift can cause detuning from the critical two-photon resonance in STIRAP. For a particle with velocity v_k, along the laser propagation direction the shift in the detuning Δ is $\Delta_{eff} = \Delta + kv_k$.The effective detuning from two-photon resonance then becomes $\delta_{\text{eff}} = (\Delta_p + kv_k) - (\Delta_s + kv_k)$. In our scheme, the two STIRAP beams are at the two photon resonance $\Delta_p = \Delta_s$, the Doppler broadening of the two-photon resonance is essentially cancelled when the two lasers beams co-propagate. Also, the Zeeman splitting for the hyperfine state F $= 1$ for a magnetic field of 1G is 0.7 MHz. This gives δ_k ($|k_p - k_s|$) = 14.6×10^{-3} , such that $\frac{\delta k}{k_p} \sim 10^{-9}$, hence the Doppler shift is negligible [79, 77, 80].

Assuming perfect optical pumping as discussed in section 2.1, the initial conditions for the above set of differential equations are $\rho_{11}(0) = 1$, $\rho_{22}(0) = \rho_{33}(0) = 0$.

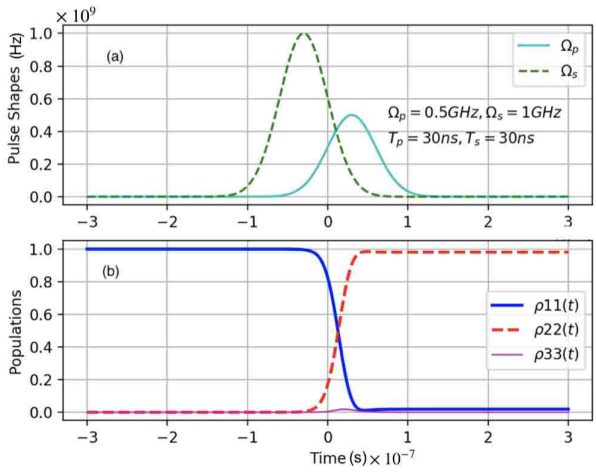

Figure 3.5. (a) The pulse shapes for the incident and coupling lasers. The counterintuitive pulse sequence is used. (b) The population evolutions of states $|1\rangle$, $|2\rangle$, and $|3\rangle$ for the counterintuitive pulse sequence, with Δ=0.5 GHz, Γ_{31}=Γ_{32}=28 MHz, $\gamma_{31} = \gamma_{32} = 2\Gamma_{31}, \gamma_{21} = 0.001\gamma_{31}$. The time width of the two pulses is *T*=30 ns. The population is transformed from level $|1\rangle$ to $|2\rangle$ with negligible population in $|3\rangle$. In order to have perfect transfer of a population from level $|1\rangle$ to $|2\rangle$, we need very high intensity lasers.

In Fig. 3.5, we consider incident photon and coupling laser pulses of time width 30 ns each. The values of the Rabi frequencies are very large for the transfer of all the atoms from level $|1\rangle$ to $|2\rangle$. However, we need only those atoms that absorb the incident photons to be transferred to level $|2\rangle$. Therefore, we can considerably reduce the Rabi frequencies of the two pulses, and as shown in Fig. 3.6, get a small probability of transfer of a single atom to level $|2\rangle$. This probability is enhanced when an ensemble of atoms is considered. For example, consider the population transfer in Fig. 3.6, which is of the order of 10^{-10}, this increases to 1% chance of transferring an atom from $|1\rangle$ to $|2\rangle$ in the presence of 10^8 atoms or approaches unity in for an ensemble of 10^{10} atoms or more.

3.4.2 Quantized STIRAP

In the quantized picture of the two-photon Raman excitation we consider both the incident photon and the coupling fields to be quantized. The fully quantized interaction Hamiltonian for a

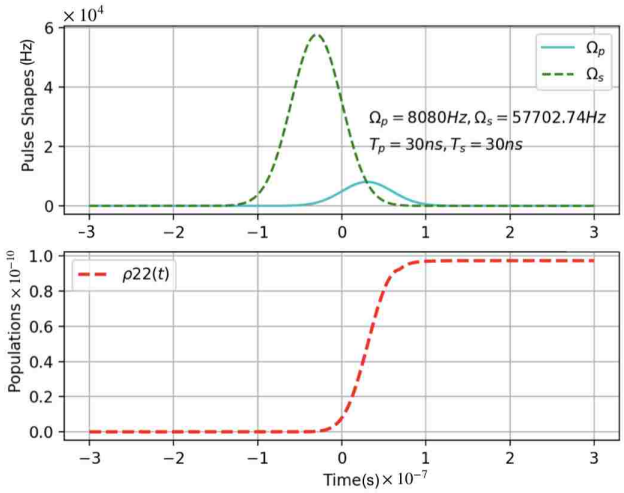

Figure 3.6. The population evolution in level $|2\rangle$ for photon and Raman pulses, with a time period of 30 ns. We have set $\Gamma_{31} = \Gamma_{32}$=28 MHz, $\gamma_{31} = \gamma_{32} = 2\Gamma_{31}, \gamma_{21} = 0.001\gamma_{31}$.

single atom in the rotating wave frame is given as,

$$\hat{H}_{int,Q} = \hbar[g_{13}\hat{a}_p\sigma_{31}e^{i\Delta t} + g_{23}\hat{a}_s\sigma_{32}e^{i\Delta t}] + h.c. \tag{3.8}$$

where $g_{13(23)}$ represents the atom-field coupling constant between levels $|1\rangle(|2\rangle)$ and $|3\rangle$. The atom-field coupling constants are given as $g_{ij} = d_{ij}\sqrt{\omega_{ij}/2\hbar\epsilon_o V}$. The eigenstates of the Hamiltonian can be written as $|1\rangle = |1_A, n_p, n_s, l\rangle$, $|3\rangle = |3_A, n_p-1, n_s, l\rangle$, and $|2\rangle = |2_A, n_p-1, n_s+1, l\rangle$, the subscript A refers to the corresponding atomic level. The number of photons in the incident photon pulse and the coupling laser are given by n_p and n_s, respectively, and l represents the photon number found in the readout laser, which we will discuss in section 2.5 .

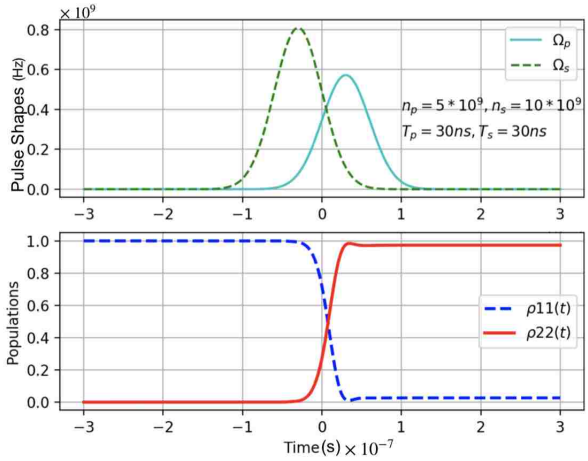

Figure 3.7. The population evolution in level $|2\rangle$ for photon and Raman pulses of time period T=30 ns. The number of photons required to complete the population transfer from $|1\rangle$ to $|2\rangle$ in the photon field are 5×10^9, and those in the Raman pulse are 10^{10}.

The equation of motions for the fully quantized interaction Hamiltonian are given as,

$$\begin{aligned}
\dot{\rho}_{11}(t) &= ig_{13}(\rho_{13}(t) - \rho^*_{13}(t))\sqrt{n_p} + \Gamma_{31}\rho_{33}(t), \\
\dot{\rho}_{13}(t) &= (i\Delta - \frac{\gamma_{13}}{2})\rho_{13}(t) + i\sqrt{n_s+1}g_{23}\rho_{12}(t), \\
&\quad - i\sqrt{n_p}g_{13}(\rho_{33}(t) - \rho_{11}(t)), \\
\dot{\rho}_{22}(t) &= -ig_{23}\sqrt{n_s+1}(\rho_{32}(t) - \rho^*_{32}(t)) + \Gamma_{32}\rho_{33}(t), \\
\dot{\rho}_{32}(t) &= -(i\Delta + \frac{\gamma_{23}}{2})\rho_{32}(t) - i\sqrt{n_p}g_{13}\rho_{12}(t), \\
&\quad + i\sqrt{n_s+1}g_{23}(\rho_{33}(t) - \rho_{22}(t)).
\end{aligned} \tag{3.9}$$

In Fig. 3.7 we plot the population evolution of levels $|1\rangle$, and $|2\rangle$, for a counter-intuitive pulse sequence of incident photon fields and the coupling laser. Here, we find that the probability of the atom being excited to level $|2\rangle$ is unity if both the incident and coupling fields contain a large number of photons. This implies that we cannot use this technique for a single or few photon detection.

Since, we want only those atoms to be transferred to level $|2\rangle$ that absorb the incident photons, we do not need a perfect population transfer from $|1\rangle$ to $|2\rangle$. In Fig 3.8. we consider the case of

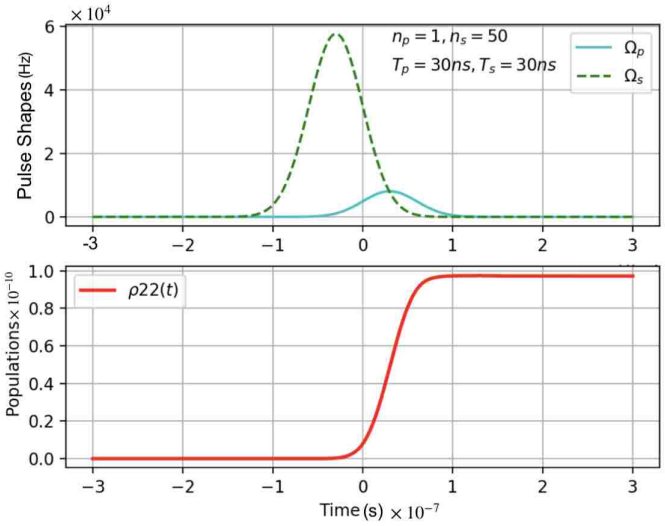

Figure 3.8. The population evolution for single-photon pulse and Raman pulse with 50 photons; both pulses have a time period of 30 ns. The value of the atom-field coupling, is given as, g_{13}=4040.83 Hz, g_{23}=4040.771 Hz. The decay rates $\Gamma_{31} = \Gamma_{32}$=28 MHz, $\gamma_{31} = \gamma_{32} = 2\Gamma_{31}, \gamma_{21} = 0.001\gamma_{31}$.

a single incident photon and a coupling field with only 50 photons. Both the fields an have equal time duration of 30 ns. We find that the probability of transferring the single atom from $|1\rangle$ to $|2\rangle$ is only 10^{-10}. This number can be enhanced when we consider an ensemble containing $10^8 - 10^{10}$ atoms.

Before wrapping up this section on STIRAP, I want to briefly mention another variant on STIRAP known as fractional STIRAP [81]. When the population transfer is partial and there exists coherent superposition of the wave-fucntion between the initial and final states via the intermediate states in the presence of both P, and S fields, the process is known as fractional STIRAP. It can be used in the production of two-qubit quantum states. Another application of STIRAP is in quantum algorithms [82]. Here, the authors showed that fractional STIRAP can be used to implement Grover's algorithm adiabatically and achieve the same Grover's speed up.

STIRAP is a promising technique that can be harnessed for applications in quantum information processing. It is resilient to some type of decoherence. However, there are still challenges in the process. One big challenge is producing high fidelity quantum gates with an efficiency of

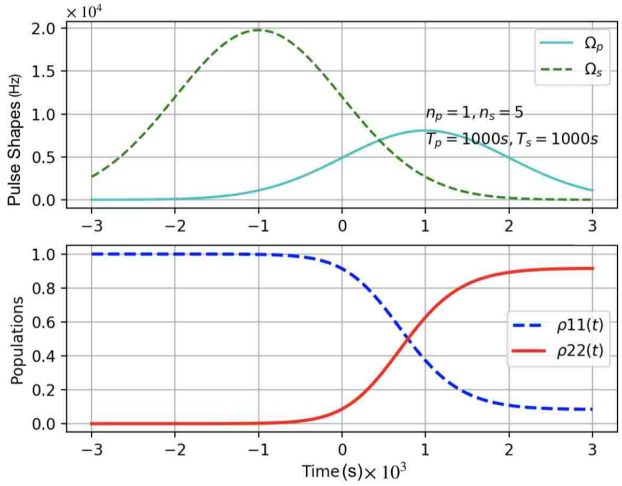

Figure 3.9. The population evolution for single photon pulse, and Raman pulse with 5 photons, both pulses have a time period of 1000 s. The value of the atom-field coupling, is given as, g_{13}=4040.83 Hz, g_{23}=4040.771 Hz. The decay rates $\Gamma_{31} = \Gamma_{32}$=28 MHz, $\gamma_{31} = \gamma_{32} = 2\Gamma_{31}, \gamma_{21} = 0.001\gamma_{31}$.

$\sim 95\%$. STIRAP can have applications in gate operation and entanglement generation, given the error can be reduced within fault tolerance threshold [75].

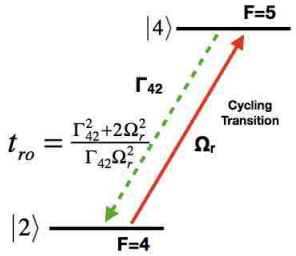

Figure 3.10. The read out laser couples only levels $|2\rangle$ and $|4\rangle$ such that only the atoms excited to level $|2\rangle$ are detected. The number of photons are counted by counting the atoms in $|2\rangle$, via the cycling transition between $|4\rangle$ and $|2\rangle$.

Another way to achieve complete population transfer from $|1\rangle$ to $|2\rangle$ for the case of single or few photon incident field is to increase the time duration of the incident and coupling pulses. We would like to point out that, there exists a hitherto hidden energy-time uncertainty in the STIRAP process. If we increase the time-period of pulses then we need less energy to drive the transitions as shown in Fig. 3.9. If we consider a pulse of time period 1000s, then the distance the pulse is distributed is 3×10^8 Km. This distance is even greater than the distance between the Earth and

the Moon which is 384400 Km! Hence it is not feasible to have pulses of such large duration.

3.5 Resonance Fluorescence

The phenomenon of resonance fluorescence has been studied for a long time. Resonance fluorescence can be described as an interaction between an atom and a strong field [25]. The plane-wave interact at near resonance, leading to inelastic scattering of the incident field. At low excitation energy the atom absorbs a photon at a certain frequency, and because of conservation of energy re-emits it at the same frequency. The spectrum of resonance fluorescence can be described into two limits i.e. weak driving field, and strong driving field. We can describe resonance fluorescence using the two-level atom equations. The metastable state $|2\rangle$ is chosen so that it can undergo a cycling transition with another atomic state $|4\rangle$. The number of atoms excited to level $|2\rangle$ are detected by employing cycling transition between $|2\rangle$ and $|4\rangle$, i.e., atoms in level $|2\rangle$ will get excited to $|4\rangle$ via the readout laser, and will spontaneously decay back only to level $|2\rangle$. The number of photons emitted will be proportional to the number of atoms in level $|2\rangle$, hence resolving the photon number in the incident radiation. The time taken for detecting a single photon using this method can be obtained by solving the equation of motion for the density matrices in steady state, and the readout laser time is given by $t_{\rm ro} = (\Gamma_{42}^2 + 2\Omega_r^2)/\Gamma_{42}\Omega_r^2$. The quantized version of resonance fluorescence yields the same steady state result, except that the Rabi frequency is $\Omega_r = 2g_r\sqrt{l}$, where g_r represents the coupling constant and l is the number of photons in the readout laser. The numerical value of $t_{\rm ro}$ is 0.052 μs for ^{133}Cs atoms.

3.6 Conclusion

In this paper we have investigated the atom-based PNRDs in detail. We have analyzed both the classical and quantum models for STIRAP. We considered the case of single atom and found that sufficiently strong probe and coupling lasers are required to transfer a single atom from the ground state to the metastable state with probability one. Therefore, an extremely weak probe pulse consisting of one or few photons cannot suffice to excite the population in the ground state to the metastable state. In other words the probability to excite a single atom to the metastable state is

extremely small. However, this probability can be enhanced if we consider an ensemble of atoms since we need only those atoms excited that absorb the incident photons, to be able to resolve photon-number at the read-out stage. This enables the use of low-intensity laser pulses. Also, there exists a trade off between the magnitude of Rabi frequencies of the probe and coupling lasers and the pulse duration. If the pulse duration increases then the magnitude of the Rabi frequencies decreases, and vice-versa. Large duration pulses imply photon wave packet spread out over large distances, which is not a desirable feature. Another source of having false photon detections (dark counts) can be due to imperfect optical pumping, i.e. if some atoms still remain in the metastable state at the initialization stage. Hence based on our analysis, if we can have an ensemble of atoms at the STIRAP stage, and implement complete optical pumping, the above technique can be used to resolve photon number at room temperature.

CHAPTER 4
THRESHOLDED QUANTUM LIDAR – EXPLOITING PHOTON-NUMBER-RESOLVING DETECTION

4.1 Introduction

Electromagnetic radiation is regularly used for measuring and sensing the physical world. One particular sensing method, namely, laser range-finding and Light Detection and Ranging (LIDAR) is under continuous development. Light Detection and Radiation (LIDAR) is a technique used for metrology (distance measurement), and remote sensing. LIDAR is an optical based RADAR for applications that require high resolution. LIDAR is a sensing technique that projects a signal onto an object and then analyzes the reflected/scattered signal (eg. time of flight) to determine the distance from the target. LIDAR is increasingly used in the field of 3D vision [83, 84, 85], dimensional control, and airborne surveillance [86], long-range target recognition. Such applications allow lower laser power and high resolution. This has been accomplished using single-photon LIDAR for measuring time-of-flight long range target recognition [7, 87].

Increasing the range requires sensitive detectors, and more recently, single-photon detectors (SPDs) [88, 89, 90, 91],and photon-number-resolving detectors (PNRDs) [92, 93] have been used for this purpose.

It is an ongoing question what quantum optics can contribute to applications like LIDAR. It has been proven that loss, such as in rangefinders and LIDARs, eliminates most quantum effects [94, 95]. Thus, it is ineffective to use quantum states of light for those applications, rather than classical light such as coherent states [23]. However, many proven quantum effects are not a result of using quantum states, but of using quantum detection of these states. For example, Bell-inequality violations are commonly attributed to the use of entangled states [96]. However, all-optical demonstrations have been done with Gaussian states, such as spontaneous parametric down-conversion

This chapter previously appeared as L. Cohen, Elisha S. Matekole, Y. Sher, D. Istrati, H. S. Eisenberg, J. P. Dowling, "Thresholded Quantum LIDAR — Exploiting Photon-Number-Resolving Detection", Phys. Rev. Lett. 123, 203601, (2019).

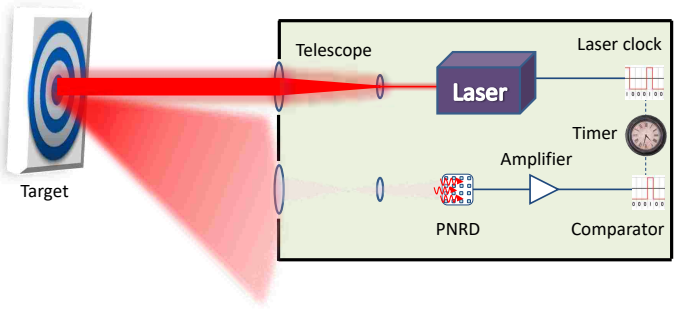

Figure 4.1. Illustration of the rangefinder system. A laser pulse is sent to a remote target and a small portion is reflected back into the device. After spatial and spectral filtering, the light is detected by a PNRD. Then, the photon number is thresholded by thresholding the voltage height. A one-bit comparator stops the timer when a voltage peak, caused by the detection of a bunch of photons, exceeds the voltage threshold.

[97]. It is well known that Bell's inequalities are satisfied when both the state and the detection are Gaussian [98]. Thus, in all-optical demonstrations, Bell-inequality violations are caused by the non-Gaussian single-photon detection [97]. Having said that, even though rangefinders and LIDARs are operated with coherent states, quantum detection strategies such as parity [23], and photon thresholding (filtering out low photon-numbers) [92] might still give a quantum advantage. In this paper, we rigorously derive the SNR improvement of threshold detection over intensity detection.

One form of laser range-finding is illustrated in Fig. 4.1. By sending short pulses of light, and recording their return time, one can measure the range to a target using the speed of light. The range-finding information can be extended to three-dimensional imaging by adding spatial resolution to the detection. Spatial resolution can be obtained by a gated camera [99], raster scanning [90] or blocking masks [89, 93]. The last method also provides compressed data acquisition, where the number of required measurements is far less than the number of image pixels, and reconstructing the signal from this measurement.

In daylight range-finding, the classical noise from solar radiation dominates the quantum noise, the latter of which is due to the photon-number fluctuations of the coherent source. Solar radiation is a blackbody radiation, and thus, single-mode sunlight has thermal photon-statistics:

$$p_{\rm th}(n) = \frac{\bar{n}_{\rm th}^n}{(\bar{n}_{\rm th}+1)^{n+1}} \tag{4.1}$$

where $p_{\rm th}(n)$ is the probability to measure *n*-photons within the coherence time, and $\bar{n}_{\rm th} = (e^{\hbar\omega/k_BT} - 1)^{-1}$ is the average photon number, $\hbar$ and k_B are the Dirac and Boltzmann constants and ω is the light frequency. The laser is a coherent light source and thus has a Poisson photon distribution:

$$p_{\rm p}(n) = e^{-\bar{n}_{\rm p}} \frac{\bar{n}_{\rm p}^n}{n!}\,, \tag{4.2}$$

where $\bar{n}_{\rm p}$ is the average photon number. Since the solar flux is continuous, identifying the signal is equivalent to distinguishing a mixture of coherent and thermal light from thermal light alone. The mixture has mixed photon-statistics [100], $p(n) = \sum_{m=0}^{n} p_{\rm p}(m) p_{\rm th}(n-m)$ which can be written as

$$p(n) = e^{\frac{\bar{n}_{\rm p}}{x} - \bar{n}_{\rm p}} \frac{x^n}{n!} \Gamma\left(\frac{\bar{n}_{\rm p}}{x}, n+1\right)\,, \tag{4.3}$$

where $x = \bar{n}_{\rm th}/(\bar{n}_{\rm th}+1)$, and $\Gamma(y, n+1) = n! e^{-y} \sum_{m=0}^{n} (y^m/m!) = \int_y^\infty t^n e^{-t} dt$ is the incomplete gamma function.

4.2 Quantum SNR versus Classical SNR

Typically, in quantum sensing technologies, it is the shot-noise limit (SNL) that is beaten [101, 102]. While sub-SNL sensitivity can be obtained when the classical noise is negligible, it is a much harder task when the classical noise is dominant [103, 104]. Nevertheless we show that even in this regime, the SNR of quantum detection schemes can still surpass the SNR of classical detection schemes.

Let us compare the classical intensity and our quantum-thresholding detection. Here the signal is regarded as the detection output with the coherent light, and the noise with the thermal light alone. As standard intensity detection is sensitive only to the average number of detected photons, the average photon number of the thermal light alone is the noise and the sum of the average

photon-number of the two light sources is the signal. Thus, the classical SNR is

$$\mathrm{SNR_c} = \frac{\bar{n}_\mathrm{p} + \bar{n}_\mathrm{th}}{\bar{n}_\mathrm{th}} \,. \tag{4.4}$$

Threshold detection has a binary outcome; it is zero — if the detected photon number is below the threshold photon number, and one — if the detected photon number is above the threshold photon number. The signal of threshold detection is proportional to the probability of successfully exceeding the threshold when coherent light also hits the detector. The noise is proportional to the probability of exceeding the threshold when only thermal light hits the detector. These probabilities are calculated by summing all the photon-number statistics above N, the threshold photon-number. Thus, the noise is $\nu \sum_{n=N}^{\infty} p_\mathrm{th}(n) = \nu x^N$, and the signal $\nu \sum_{n=N}^{\infty} p(n) = \nu \left(1 - \sum_{n=0}^{N-1} p(n)\right)$, where ν is the number of experimental repetitions. After substituting $p(n)$, reordering the sums and summing over *n*, we are left with, $\nu \left(1 - \sum_{m=0}^{N-1} \left(1 - x^{N-m}\right) p_\mathrm{p}(m)\right)$. Using the formula of the incomplete gamma function and dividing by the noise, we get that the SNR for threshold detection is:

$$\mathrm{SNR_q} = \frac{1 - \frac{\Gamma(\bar{n}_\mathrm{p}, N)}{(N-1)!} - \frac{\Gamma(\frac{\bar{n}_\mathrm{p}}{x}, N)}{(N-1)!} e^{\frac{\bar{n}_\mathrm{p}}{x} - \bar{n}_\mathrm{p}} x^N}{x^N} \,. \tag{4.5}$$

Notice that the noise exponentially decays with the threshold number. This decay eventually gives the SNR improvement that we will see in the following.

We wish to get some insights into the expression of Eq. 4.5. First, we differentiate the SNR with respect to $\bar{n}_\mathrm{p}$,

$$\frac{\partial}{\partial \bar{n}_\mathrm{p}} \mathrm{SNR_q} = \left(\frac{1}{x} - 1\right) \frac{\Gamma(\frac{\bar{n}_\mathrm{p}}{x}, N)}{(N-1)!} e^{\frac{\bar{n}_\mathrm{p}}{x} - \bar{n}_\mathrm{p}} x^N > 0,$$

which means that the SNR is a monotonically increasing function of the coherent mean-photon number regardless of the threshold and averaged thermal photon-number. This dependence is expected, since increasing the signal intensity should increase the SNR.

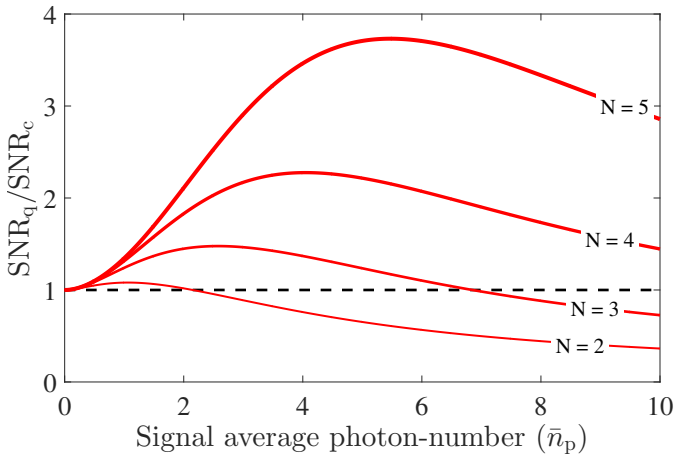

Figure 4.2. The ratio of the quantum and classical SNR for fixed thermal average photon-number of one. Thresholds of $N = 2, 3, 4, 5$ are plotted where a thicker line corresponds to a higher threshold. The dashed black line at one represents the limit, above which the quantum scheme gets a better SNR.

Next, we check the threshold dependence on photon number. The difference $[\mathrm{SNR_q}(N+1) - \mathrm{SNR_q}(N)]$ can be written as $[\sum_{n=N}^{\infty} p(n+1) - \sum_{n=N}^{\infty} p(n)x]/x^{N+1}$, where the first summation is transformed as $n \to n+1$. Now the two summations can be regrouped into one, and its argument is $(1-x)p_p(n+1)$. Thus, the SNR obeys

$$[\mathrm{SNR_q}(N+1) - \mathrm{SNR_q}(N)] = \frac{1-x}{x^{N+1}} \sum_{n=N}^{\infty} p_p(n+1) > 0\,, \tag{4.6}$$

i.e, taking larger photon-number thresholds increases the SNR for any intensity of the coherent and thermal light. In order to demonstrate the advantage of our quantum scheme, Fig. 4.2 shows the ratio of the quantum and classical SNR for a fixed averaged-thermal photon number of one. Different threshold photon numbers are plotted with different line widths.

4.3 Discussion

For many average signal and threshold photon numbers, the ratio of SNR is above one, which means that the quantum SNR exceeds the classical SNR. This improvement is a result of the difference between the signal and noise photon distribution. The thermal distribution is dominant near the low photon numbers, whereas the Poisson distribution is more dominant near the mean

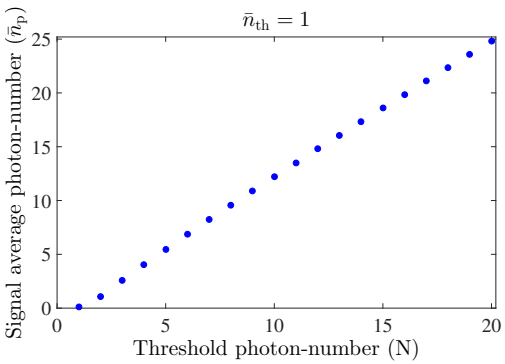

(a)

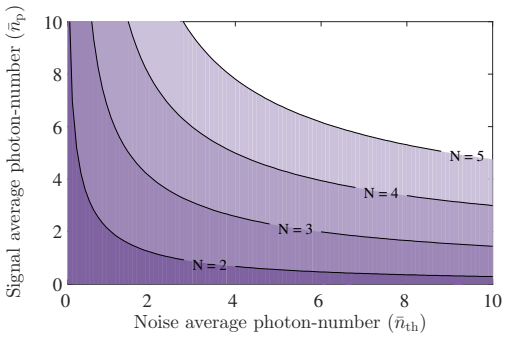

(b)

Figure 4.3. (a) The coherent light (signal) intensity that achieve the best improvement with respect to the classical detection scheme for fixed thermal average photon-number of one. (b) Parameter-space representation of the quantum improvement. The line denotes the limit of quantum improvement, where below the line the threshold detection gives higher SNR than the classical detection, for particular threshold number, N. The area under the line increases for larger threshold numbers, showing the improvement achieved by taking larger threshold.

photon number (see Fig. B1 in appendix B). By using threshold detection we exclude low photon numbers where the noise is dominant.

As shown in Eq. 4.6, the quantum SNR increases when a larger photon number threshold is used. Thus, the ratio of the two SNRs increases with the threshold, since the classical SNR is independent of the threshold. However, taking threshold much larger than the average photon number will cause substantial decrease in the successful threshold detection. Any practical application should choose the threshold photon number in accordance with this trade-off; higher threshold means higher SNR but lower successful threshold detection, lower threshold means higher successful threshold detection but lower SNR. For a practical rangefinder or LIDAR, threshold detection success should be every couple of trials. Thus, in the regime of a few detected signal photons, the best improvement is around four.

In Fig. 4.2, for every threshold there is an averaged signal-photon number where the improvement is maximal. In Fig. 4.3a, this maximum mean photon number is plotted as a function of the threshold. The improvement is maximal where the threshold is around the mean photon number. This observation can be understood by the fact that the coherent light has a more localized distribution

than the thermal light, i.e. the variance of Poisson distribution equals the mean and that of thermal distribution equals the mean square. Thus, if the threshold is well-above the mean photon number of the signal, the detection loses most of the signal, and if it is well below the mean photon number, it is contaminated with noise without gaining signal.

As seen in Fig. 4.2, the quantum SNR does not always exceed the classical SNR. Figure 4.3b is a parameter-space plot, showing the parameters under which quantum detection is superior. Below the line (the darker area) threshold detection presents better SNR. As expected from Eq. 4.6, the area, where quantum detection outperforms the classical detection, grows as the threshold number is increased. We note that the curved point of each graph holds $N \approx \bar{n}_{\mathrm{th}}$. This fact may help to set the threshold as in most applications the noise intensity is approximately known or can be easily measured.

In the same manner, it seems from the right bottom side of Fig. 4.3b that threshold detection always gives better results where the noise is high and the signal is low. Thus, in high-noise low-signal regime, threshold detection is definitely preferable.

We note that the average photon numbers ($\bar{n}_{\mathrm{p}},\ \bar{n}_{\mathrm{th}}$) are the measured averages, i.e. we already account for the loss of the detector. Other effects of the PNRD were considered, based on our PNRD model [105], and those effects changed the results slightly. In particular, nonlinear loss has low effect on the results, because we limited our signal to a few photons where the nonlinear loss is negligible (see Fig. B2 in appendix B).

While Eq. 4.5 and Fig. 4.2 show the average results for the quantum SNR and SNR ratio (i.e. infinite ensemble of measurement samplings), most applications may sample the signal only a few times. We simulate multi-target range-finding to show the improvement with a finite number of samplings. In the simulation, the time is divided to 50 time-bins, where the thermal noise is fixed with $\bar{n}_{\mathrm{th}} = 1$. Each time-bin contains thermally distributed noise photons. Four targets are simulated by adding photons with a Poisson distribution of $0.5\,, 1\,, 3$ and 10 mean photon numbers at times of $10, 20, 30$ and 40, respectively. The simulation runs 100 and 10,000 times, where the

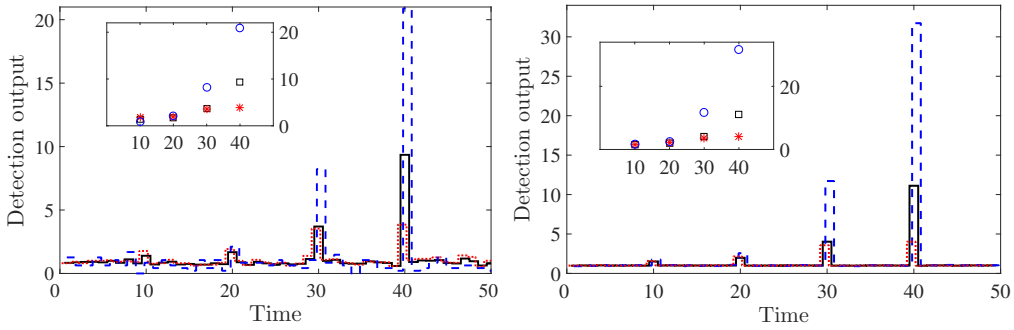

(a) (b)

Figure 4.4. The simulation results comparing intensity detection and thresholding detection for 100 (a) and 10,000 (b) repetitions. The intensity detection is plotted with solid black line, two-photon thresholding with red dotted line, and five-photon thresholding with blue dashed line. The three graphs are slightly shifted, for visual purposes. The signal height is normalized such that the noise average is one. The inset shows the same comparison only for the time bins with the coherent photons. The intensity detection is plotted with black boxes, two-photon thresholding with red asterisks, and five-photon thresholding with blue circles.

former is equivalent to less-than-a-second operation of a typical rangefinder.

The simulation results are shown in Fig. 4.4. Naturally, the effect of low sampling is larger fluctuations, which can be seen in Fig. 4.4a, especially for five-photon thresholding where the detection rate is low. The weak target with $\bar{n}_{\mathrm{p}} = 0.5$ is detected well with two-photon thresholding but not detected at all with five-photon thresholding. This effect is again due to the detection rate. When the number of simulation repetitions is increased, the ratio of the SNR approaches the values of Fig. 4.2. For the target with $\bar{n}_{\mathrm{p}} = 10$, the output of five-photon thresholding is 31.7 and of intensity is 11.1. As the noise is normalized to one, the ratio of the SNR is just $\frac{31.7}{11.1} = 2.86$, which is exactly the result of Fig. 4.2. For the weak target with $\bar{n}_{\mathrm{p}} = 0.5$, the output of two-photon thresholding is 1.58, of five-photon thresholding is 1.77 and of intensity is 1.51, which gives SNR ratio of 1.04 and 1.17 where 1.05 and 1.10 are deduced from Fig. 4.2.

We propose to implement the threshold detector with PNRDs. There may be other implementation methods, such as N-photon-ionization processes. Additionally, other detection protocols using PNRDs may give higher gain of the localized photon distribution, and thus, better SNR improvement. Examples include exact photon-number detection (i.e. projecting on a specific Fock

state) [106] and a range of photon-number detection. These protocols require knowledge about the signal intensity and are suited to applications with known signal intensity. Threshold detection does not require knowledge about the signal intensity, and thus is suited to applications like range-finding and LIDAR, where the signal intensity is a priory unknown. The next-gen LIDAR technology is focusing on autonomous driving with real-time discernment of signals. In other words, the next-generation LIDAR would have to distinguish between different signals in extremely fast response time and high efficiency [107].

4.4 Conclusion

We have shown that PNRDs can provide better SNR by thresholding the photon number instead of directly detecting intensity. Additionally, we have theoretically tested our results for imperfect PNRDs, including nonlinear loss. This leads to a slightly lower SNR. The method seems to always improve the SNR in the high-noise low-signal regime. The method has been implemented in rangefinders and LIDARs, but can also be used for any application with low-signal detection in the presence of thermal noise.

APPENDIX A
ROOM-TEMPERATURE PHOTON-NUMBER-RESOLVED DETECTION USING A TWO-MODE SQUEEZER

The expressions for the variance in intensity-intensity correlation signal $\Delta C^2 = \langle \hat{C}^2 \rangle - \langle \hat{C} \rangle^2$ and signal- to-noise ratio are given by the following equations,

$$
\begin{aligned}
\Delta C^2 = {} & N^2\alpha^2(1+\sinh(r)^2)^4 + (1+\sinh(r)^2)^3\sinh(r)^2 + 3N(1+\sinh(r)^2)^3\sinh(r)^2 \\
& + 3N^2(1+\sinh(r)^2)^3\sinh(r)^2 + N^3(1+\sinh(r)^2)^3\sinh(r)^2 \\
& + 7\alpha^2(1+\sinh(r)^2)^3\sinh(r)^2 + 19N\alpha^2(1+\sinh(r)^2)^3\sinh(r)^2 \\
& + 11N^2\alpha^2(1+\sinh(r)^2)^3\sinh(r)^2 + 2N^3\alpha^2(1+\sinh(r)^2)^3\sinh(r)^2 \\
& + 6\alpha^4(1+\sinh(r)^2)^3\sinh(r)^2 \\
& + 13N\alpha^4(1+\sinh(r)^2)^3\sinh(r)^2 + 4N^2\alpha^4(1+\sinh(r)^2)^3\sinh(r)^2 \\
& + \alpha^6(1+\sinh(r)^2)^3\sinh(r)^2 + 2N\alpha^6(1+\sinh(r)^2)^3\sinh(r)^2 \\
& + 10(1+\sinh(r)^2)^2\sinh(r)^4 + 20N(1+\sinh(r)^2)^2\sinh(r)^4 \\
& + 12N^2(1+\sinh(r)^2)^2\sinh(r)^4 + 2N^3(1+\sinh(r)^2)^2\sinh(r)^4 \\
& + 43\alpha^2(1+\sinh(r)^2)^2\sinh(r)^4 + 68N\alpha^2(1+\sinh(r)^2)^2\sinh(r)^4 \\
& + 32N^2\alpha^2(1+\sinh(r)^2)^2\sinh(r)^4 + 4N^3\alpha^2(1+\sinh(r)^2)^2\sinh(r)^4 \\
& + 32\alpha^4(1+\sinh(r)^2)^2\sinh(r)^4 + 36N\alpha^4(1+\sinh(r)^2)^2\sinh(r)^4 \\
& + 10N^2\alpha^4(1+\sinh(r)^2)^2\sinh(r)^4 \\
& + 6\alpha^6(1+\sinh(r)^2)^2\sinh(r)^4 + 4N\alpha^6(1+\sinh(r)^2)^2\sinh(r)^4 \\
& + 9(1+\sinh(r)^2)\sinh(r)^6 + 15N(1+\sinh(r)^2)\sinh(r)^6 \\
& + 7N^2(1+\sinh(r)^2)\sinh(r)^6 + N^3(1+\sinh(r)^2)\sinh(r)^6 \\
& + 29\alpha^2(1+\sinh(r)^2)\sinh(r)^6 + 47N\alpha^2(1+\sinh(r)^2)\sinh(r)^6 \\
& + 19N^2\alpha^2(1+\sinh(r)^2)\sinh(r)^6 \\
& + 2N^3\alpha^2(1+\sinh(r)^2)\sinh(r)^6 + 14\alpha^4(1+\sinh(r)^2)\sinh(r)^6 \\
& + 21N\alpha^4(1+\sinh(r)^2)\sinh(r)^6 + 4N^2\alpha^4(1+\sinh(r)^2)\sinh(r)^6 \\
& + \alpha^6(1+\sinh(r)^2)\sinh(r)^6 + 2N\alpha^6(1+\sinh(r)^2)\sinh(r)^6 \\
& + \alpha^2\sinh(r)^8 + 2N\alpha^2\sinh(r)^8 + N^2\alpha^2\sinh(r)^8, \qquad \text{(A.1)}
\end{aligned}
$$

$$
\begin{aligned}
\mathrm{SNR} = {} & (\eta^2(N\alpha^2(1+\sinh(r)^2)^2 + ((1+N)^2 + (3+2N)\alpha^2 + \alpha^4)(1+\sinh(r)^2)\sinh(r)^2 \\
& + (1+N)(1+\alpha^2)\sinh(r)^4))/ \\
& ((1-\eta)^2\eta^2(N\alpha^2(1+\sinh(r)^2)^2 + ((1+N)^2 + (3+2N)\alpha^2 + \alpha^4)(1+\sinh(r)^2)\sinh(r)^2 \\
& + (1+N)(1+\alpha^2)\sinh(r)^4) - \eta^4(N\alpha^2(1+\sinh(r)^2)^2 \\
& + ((1+N)^2 + (3+2N)\alpha^2 + \alpha^4)(1+\sinh(r)^2)\sinh(r)^2 \\
& + (1+N)(1+\alpha^2)\sinh(r)^4)^2 + (1-\eta)\eta^3(N(\alpha^2+\alpha^4)(1+\sinh(r)^2)^3 + (2\alpha^2 + N^2\alpha^2 \\
& + 2N(1+N)\alpha^2 + 4\alpha^4 + \alpha^6 + N(1+N)(1+\alpha^2) + N(\alpha^2+2\alpha^4) \\
& + (1+N)(1+5\alpha^2+2\alpha^4))(1+\sinh(r)^2)^2\sinh(r)^2 + (N(1+N)^2 + (N^2 + N(1+N))\alpha^2 \\
& + (1+N)(3+2N)(1+\alpha^2) + N(2\alpha^2+\alpha^4) \\
& + (1+N)(1+7\alpha^2+3\alpha^4))(1+\sinh(r)^2)\sinh(r)^4 + (1+N)^2(1+\alpha^2)\sinh(r)^6) \\
& + (1-\eta)\eta^3(N^2\alpha^2(1+\sinh(r)^2)^3 + (N^2(1+N) + (-1+N)N\alpha^2 + N^2\alpha^2 + N(1+N)(1+\alpha^2) \\
& + (1+N)^2(1+\alpha^2) + N(\alpha^2+\alpha^4) + 2N(2\alpha^2+\alpha^4) + (1+N)(2\alpha^2+\alpha^4))(1+\sinh(r)^2)^2\sinh(r)^2 \\
& + (4\alpha^2 + N(1+N)\alpha^2 + 5\alpha^4 + \alpha^6 + 2N(1+N)(1+\alpha^2) + (1+N)^2(1+\alpha^2) \\
& + N(\alpha^2+\alpha^4) + N(2\alpha^2+\alpha^4) + (1+N)(1+3\alpha^2+\alpha^4) \\
& + (1+N)(2+4\alpha^2+\alpha^4))(1+\sinh(r)^2)\sinh(r)^4 + (1+N)(1+3\alpha^2+\alpha^4)\sinh(r)^6) \\
& + \eta^4(N^2(\alpha^2+\alpha^4)(1+\sinh(r)^2)^4 + ((2+7N)\alpha^2 + (4+15N)\alpha^4 \\
& + (1+4N)\alpha^6)(1+\sinh(r)^2)^3\sinh(r)^2 + (N^3\alpha^2 + 2N^2(1+N)\alpha^2 \\
& + N^2(1+N)(1+\alpha^2))(1+\sinh(r)^2)^3\sinh(r)^2 + (1+5\alpha^2+2\alpha^4+2N^2(1+6\alpha^2+4\alpha^4) \\
& + N(3+14\alpha^2+4\alpha^4))(1+\sinh(r)^2)^3\sinh(r)^2 + N^2(1+N)^2(1+\sinh(r)^2)^2\sinh(r)^4 \\
& + (3+3N+27\alpha^2+30N\alpha^2+24\alpha^4+36N\alpha^4+4\alpha^6 \\
& + 8N\alpha^6)(1+\sinh(r)^2)^2\sinh(r)^4 + (4\alpha^2+14\alpha^4+8\alpha^6+\alpha^8)(1+\sinh(r)^2)^2\sinh(r)^4 \\
& + (1+2N)(3(1+\alpha^2) + N^2(2+4\alpha^2) + N(5+4\alpha^2))(1+\sinh(r)^2)^2\sinh(r)^4 \\
& + ((-1+N)N\alpha^4 + (N^2+2N(1+N))(\alpha^2+\alpha^4) \\
& + (2N^2 + 6N(1+N) + 2(1+N)^2)(2\alpha^2+\alpha^4) + (2N(1+N) + (1+N)^2)(1+3\alpha^2+\alpha^4) \\
& + (1+N)(2+N)(2+4\alpha^2+\alpha^4))(1+\sinh(r)^2)^2\sinh(r)^4 + (N(1+N)^2\alpha^2 + 2N(1+N)^2(1+\alpha^2) \\
& + (1+N)^3(1+\alpha^2))(1+\sinh(r)^2)\sinh(r)^6 + ((N^2+N(1+N))(3\alpha^2+2\alpha^4) + ((1+N)^2 \\
& + (1+N)(2+N))(3+7\alpha^2+2\alpha^4))(1+\sinh(r)^2)\sinh(r)^6 + (N(4\alpha^2+5\alpha^4+\alpha^6) \\
& + 2(1+N)(4\alpha^2+5\alpha^4+\alpha^6) + (1+N)(1+7\alpha^2+6\alpha^4+\alpha^6))(1+\sinh(r)^2)\sinh(r)^6 \\
& + (1+N)^2(1+3\alpha^2+\alpha^4)\sinh(r)^8))))^{1/2}. \qquad \text{(A.2)}
\end{aligned}
$$

APPENDIX B
THRESHOLDED QUANTUM LIDAR

B.1 Photon Distribution

In order to show the difference in the photon number distribution, figure B.1 shows the thermal and Poisson statistics for average photon number of two. As mentioned in the main text, the thermal distribution is dominant near the low photon numbers, i.e. most of the time, a low photon number will be detected. On the other hand, Poisson distribution is dominant near the mean photon number, i.e. most of the time, a photon number around the average will be detected.

B.2 Imperfect Detector

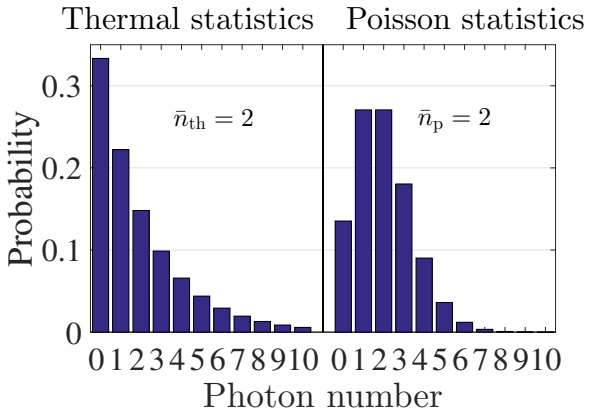

Figure B.1. Thermal (left) and Poisson (right) photon-number distributions.

In the main text, we showed the results of the SNR improvement assuming the detector has no distortion effects for example dark counts, except of non-unity detection efficiency. Here Fig. B.2 shows the results after including these effects of the detector.

In order to use practical numbers, a specific detector (silicon photomultiplier of *Hamamatsu Photonics*, model No. S10362-11-100U) [108, 109] has been chosen as the PNRD. We use our detector model to calculate the photon statistics after the distortion effects[105] (see caption of Fig. B.2). The parameters for the detector effects are chosen based on parameters from previous experiments[100].

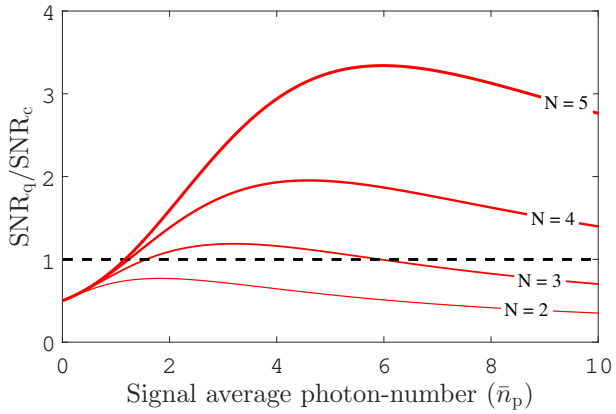

Figure B.2. The ratio of the quantum and classical SNR for fixed thermal average photon-number of one and after including the effects of the PNRD. Thresholds of $N = 2, 3, 4, 5$ are plotted where a thicker line corresponds to a higher threshold. The dashed black line at one represents the limit, above which the quantum scheme gets a better SNR. The dark count parameter is 1.4×10^{-5}, the cross-talk parameter is 0.048, and the number of detector elements is 100 (see Ref. [100, 105] for more information).

Qualitatively, the results in Fig. B.2 look the same as Fig. 2 of the main text. Quantitatively, one can notice a slight reduction in the SNR ratio. This is mainly caused by the increase of the average photon number of the thermal light from one to 1.15, due to the effects of the PNRD. In particular, the finite number of detector elements, which in principle causes lower detection efficiency for higher photon number (usually called nonlinear loss) has a small effect on the results. It is due to the relatively low photon number compared to the number of elements, which is about an order of magnitude less, while nonlinear loss is noticeable where the photon number is above 20 percent of the element number [110].

B.3 Simulation Parameters

The simulations (see Fig. 4 in the main text) were run with dimensionless parameters. Reincorporating the units can be done as follows:

The frequency, temperature and average thermal photon number are connected via the Planck formula: $\bar{n} = (e^{\hbar\omega/k_B T} - 1)^{-1}$ [111]. To get an average thermal photon number of one, one should take the temperature of the sun (5770 Kelvin) and IR laser light source with frequency of 542 THz.

The time bin of the chosen PNRD is around 1 nanosecond (ns). Therefore, the times of flight

in the simulation are 10 ns, 20 ns, 30 ns and 40 ns. The range is related to the time of flight by $R = ct/2$, where R is the range, c is the speed of light, and t is the time of flight. Thus, the target ranges in the simulation are 1.5 m, 3.0 m, 4.5 m, and 6.0 m.

APPENDIX C
COPYRIGHT INFORMATION

American Physical Society
Reuse and Permissions License

18-Feb-2020

This license agreement between the American Physical Society ("APS") and Elisha Siddiqui Matekole ("You") consists of your license details and the terms and conditions provided by the American Physical Society and SciPris.

Licensed Content Information

License Number:	**RNP/20/FEB/022908**
License date:	18-Feb-2020
DOI:	10.1103/PhysRevA.96.053815
Title:	Room-temperature photon-number-resolved detection using a two-mode squeezer
Author:	Elisha S. Matekole et al.
Publication:	Physical Review A
Publisher:	American Physical Society
Cost:	USD $ 0.00

Request Details

Does your reuse require significant modifications: No

Specify intended distribution locations:	United States
Reuse Category:	Reuse in a thesis/dissertation
Requestor Type:	Author of requested content
Items for Reuse:	Whole Article
Format for Reuse:	Electronic

Information about New Publication:

University/Publisher:	Louisiana State University
Title of dissertation/thesis:	Novel Photon-detector Models for Enhanced Quantum Information Processing
Author(s):	Elisha Siddiqui Matekole
Expected completion date:	May. 2020

License Requestor Information

Name:	Elisha Siddiqui Matekole
Affiliation:	Individual
Email Id:	esiddi1@lsu.edu
Country:	United States

American Physical Society
Reuse and Permissions License

18-Feb-2020

This license agreement between the American Physical Society ("APS") and Elisha Siddiqui Matekole ("You") consists of your license details and the terms and conditions provided by the American Physical Society and SciPris.

Licensed Content Information

License Number:	**RNP/20/FEB/022908**
License date:	18-Feb-2020
DOI:	10.1103/PhysRevA.96.053815
Title:	Room-temperature photon-number-resolved detection using a two-mode squeezer
Author:	Elisha S. Matekole et al.
Publication:	Physical Review A
Publisher:	American Physical Society
Cost:	USD $ 0.00

Request Details

Does your reuse require significant modifications: No

Specify intended distribution locations:	United States
Reuse Category:	Reuse in a thesis/dissertation
Requestor Type:	Author of requested content
Items for Reuse:	Whole Article
Format for Reuse:	Electronic

Information about New Publication:

University/Publisher:	Louisiana State University
Title of dissertation/thesis:	Novel Photon-detector Models for Enhanced Quantum Information Processing
Author(s):	Elisha Siddiqui Matekole
Expected completion date:	May. 2020

License Requestor Information

Name:	Elisha Siddiqui Matekole
Affiliation:	Individual
Email Id:	esiddi1@lsu.edu
Country:	United States

American Physical Society
Reuse and Permissions License

18-Feb-2020

This license agreement between the American Physical Society ("APS") and Elisha Siddiqui Matekole ("You") consists of your license details and the terms and conditions provided by the American Physical Society and SciPris.

Licensed Content Information

License Number:	**RNP/20/FEB/022907**
License date:	18-Feb-2020
DOI:	10.1103/PhysRevA.98.033829
Title:	Limits to atom-vapor-based room-temperature photon-number-resolving detection
Author:	Elisha S. Matekole, Hwang Lee, and Jonathan P. Dowling
Publication:	Physical Review A
Publisher:	American Physical Society
Cost:	USD $ 0.00

Request Details

Does your reuse require significant modifications: No

Specify intended distribution locations:	United States
Reuse Category:	Reuse in a thesis/dissertation
Requestor Type:	Author of requested content
Items for Reuse:	Whole Article
Format for Reuse:	Electronic

Information about New Publication:

University/Publisher:	Louisiana State University
Title of dissertation/thesis:	Novel Photon-detector Models for Enhanced Quantum Information Processing
Author(s):	Elisha Siddiqui Matekole
Expected completion date:	May. 2020

License Requestor Information

Name:	Elisha Siddiqui Matekole
Affiliation:	Individual
Email Id:	esiddi1@lsu.edu
Country:	United States

REFERENCES

[1] T. D. Ladd, F. Jelezko, R. Laflamme, Y. Nakamura, C. Monroe, and J. L. O'Brien, "Quantum computers," *Nature*, vol. 464, no. 7285, pp. 45–53, 2010.

[2] H. J. Kimble, "The quantum internet," *Nature*, vol. 453, no. 7198, pp. 1023–1030, 2008.

[3] A. Boaron, G. Boso, D. Rusca, C. Vulliez, C. Autebert, M. Caloz, M. Perrenoud, G. Gras, F. Bussières, M.-J. Li, D. Nolan, A. Martin, and H. Zbinden, "Secure quantum key distribution over 421 km of optical fiber," *Phys. Rev. Lett.*, vol. 121, p. 190502, Nov 2018.

[4] S. Polyakov, A. Migdall, J. Fan, and J. Bienfang, *Single-Photon Generation and Detection*. Elsevier Inc., 2013.

[5] M. Fiorentino, C. Santori, S. M. Spillane, R. G. Beausoleil, and W. J. Munro, "Secure self-calibrating quantum random-bit generator," *Phys. Rev. A*, vol. 75, p. 032334, Mar 2007.

[6] I. J. Owens, R. J. Hughes, and J. E. Nordholt, "Entangled quantum-key-distribution randomness," *Phys. Rev. A*, vol. 78, p. 022307, Aug 2008.

[7] R. H. Hadfield, "Single-photon detectors for optical quantum information applications," *Nature Photonics*, vol. 3, no. 12, pp. 696–705, 2009.

[8] C. J. Chunnilall, I. P. Degiovanni, S. Kück, I. Müller, and A. G. Sinclair, "Metrology of single-photon sources and detectors: a review," *Optical Engineering*, vol. 53, no. 8, pp. 1 – 17, 2014.

[9] A. K. Ekert, "Quantum cryptography based on bell's theorem," *Phys. Rev. Lett.*, vol. 67, pp. 661–663, Aug 1991.

[10] C. H. Bennett, "Quantum cryptography using any two nonorthogonal states," *Phys. Rev. Lett.*, vol. 68, pp. 3121–3124, May 1992.

[11] Y. Zhao, B. Qi, X. Ma, H.-K. Lo, and L. Qian, "Experimental quantum key distribution with decoy states," *Phys. Rev. Lett.*, vol. 96, p. 070502, Feb 2006.

[12] C. Simon, H. de Riedmatten, M. Afzelius, N. Sangouard, H. Zbinden, and N. Gisin, "Quantum repeaters with photon pair sources and multimode memories," *Phys. Rev. Lett.*, vol. 98, p. 190503, May 2007.

[13] N. Sangouard, C. Simon, H. de Riedmatten, and N. Gisin, "Quantum repeaters based on atomic ensembles and linear optics," *Rev. Mod. Phys.*, vol. 83, pp. 33–80, Mar 2011.

[14] C. H. Bennett, G. Brassard, C. Crépeau, R. Jozsa, A. Peres, and W. K. Wootters, "Teleporting an unknown quantum state via dual classical and einstein-podolsky-rosen channels," *Phys. Rev. Lett.*, vol. 70, pp. 1895–1899, Mar 1993.

[15] D. J. Brod, E. F. Galvão, A. Crespi, R. Osellame, N. Spagnolo, and F. Sciarrino, "Photonic implementation of boson sampling: a review," *Advanced Photonics*, vol. 1, no. 3, pp. 1–14, 2019.

[16] L. K. Shalm, E. Meyer-Scott, B. G. Christensen, P. Bierhorst, M. A. Wayne, M. J. Stevens, T. Gerrits, S. Glancy, D. R. Hamel, M. S. Allman, K. J. Coakley, S. D. Dyer, C. Hodge, A. E. Lita, V. B. Verma, C. Lambrocco, E. Tortorici, A. L. Migdall, Y. Zhang, D. R. Kumor, W. H. Farr, F. Marsili, M. D. Shaw, J. A. Stern, C. Abellán, W. Amaya, V. Pruneri, T. Jennewein, M. W. Mitchell, P. G. Kwiat, J. C. Bienfang, R. P. Mirin, E. Knill, and S. W. Nam, "Strong loophole-free test of local realism," *Phys. Rev. Lett.*, vol. 115, p. 250402, Dec 2015.

[17] A. E. Lita, A. J. Miller, and S. Nam, "Counting near-infrared single-photons with 95% efficiency," *Optical Express*, vol. 16, p. 3032, 2008.

[18] A. E. Lita, A. J. Miller, and S. Nam, "Energy collection efficiency of tungsten transition-edge sensors in the near-infrared," *Journal of Low Temperature Physics*, vol. 151, pp. 125–130, Apr 2008.

[19] B. Calkins, P. L. Mennea, A. E. Lita, B. J. Metcalf, W. S. Kolthammer, A. Lamas-Linares, J. B. Spring, P. C. Humphreys, R. P. Mirin, J. C. Gates, P. G. R. Smith, I. A. Walmsley, T. Gerrits, and S. W. Nam, "High quantum-efficiency photon-number-resolving detector for photonic on-chip information processing," *Opt. Express*, vol. 21, pp. 22657–22670, Sep 2013.

[20] L. Cohen, E. S. Matekole, Y. Sher, D. Istrati, H. S. Eisenberg, and J. P. Dowling, "Thresholded quantum lidar: Exploiting photon-number-resolving detection," *Phys. Rev. Lett.*, vol. 123, p. 203601, Nov 2019.

[21] Z. Bao, Y. Liang, Z. Wang, Z. Li, E. Wu, G. Wu, and H. Zeng, "Laser ranging at few-photon level by photon-number-resolving detection," *Appl. Opt.*, vol. 53, pp. 3908–3912, Jun 2014.

[22] Y. Sher, L. Cohen, D. Istrati, and H. S. Eisenberg, "Low intensity LiDAR using compressed sensing and a photon number resolving detector," in *Emerging Digital Micromirror Device Based Systems and Applications X* (M. R. Douglass and B. L. Lee, eds.), vol. 10546, pp. 70 – 76, International Society for Optics and Photonics, SPIE, 2018.

[23] K. Jiang, H. Lee, C. C. Gerry, and J. P. Dowling, "Super-resolving quantum radar: Coherent-state sources with homodyne detection suffice to beat the diffraction limit," *Journal of Applied Physics*, vol. 114, no. 19, p. 193102, 2013.

[24] C. C. Gerry and P. L. Knight, *Introductory Quantum Optics*. Cambridge University Press, Cambridge U.K., 2005.

[25] M. O. Scully and M. S. Zubairy, *Quantum Optics*. Cambridge University Press, 1997.

[26] E. Knill, R. Laflamme, and G. Milburn, "A scheme for efficient quantum computation with linear optics," *Nature*, vol. 409, pp. 46–52, 2001.

[27] P. Kok, W. J. Munro, K. Nemoto, T. C. Ralph, J. P. Dowling, and G. J. Milburn, "Linear optical quantum computing," *Rev. Mod. Phys.*, vol. 79, p. 135, 2007.

[28] C. Simon, H. de Riedmatten, M. Afzelius, N. Sangouard, H. Zbinden, and N. Gisin, "Quantum repeaters with photon pair sources and multimode memories," *Phys. Rev. Lett.*, vol. 98, p. 190503, May 2007.

[29] A. Scherer, R. B. Howard, B. C. Sanders, and W. Tittel, "Quantum states prepared by realistic entanglement swapping," *Phys. Rev. A*, vol. 80, p. 062310, Dec 2009.

[30] C. Śliwa and K. Banaszek, "Conditional preparation of maximal polarization entanglement," *Phys. Rev. A*, vol. 67, p. 030101, Mar 2003.

[31] A. J. Shields, "Semiconductor quantum light sources," *Nature Photonics*, vol. 1, pp. 215–223, 2007.

[32] D. Lincoln, "A large statistics study of the performance and yields of generation-6 vlpcs (histe-vi)," *Nucl.Instrum.Meth. A*, vol. 453, pp. 177–181, 2000.

[33] E. Waks, E. Diamanti, B. C. Sanders, S. D. Bartlett, and Y. Yamamoto, "Direct observation of nonclassical photon statistics in parametric down-conversion," *Phys. Rev. Lett.*, vol. 92, p. 113602, Mar 2004.

[34] C. F. Wildfeuer, A. J. Pearlman, J. Chen, J. Fan, A. Migdall, and J. P. Dowling, "Resolution and sensitivity of a fabry-perot interferometer with a photon-number-resolving detector," *Phys. Rev. A*, vol. 80, p. 043822, Oct 2009.

[35] B. Kühn and W. Vogel, "Unbalanced homodyne correlation measurements," *Phys. Rev. Lett.*, vol. 116, p. 163603, Apr 2016.

[36] G. Brassard, N. Lütkenhaus, T. Mor, and B. C. Sanders, "Limitations on practical quantum cryptography," *Phys. Rev. Lett.*, vol. 85, pp. 1330–1333, Aug 2000.

[37] S. W. N. Aaron J. Miller and J. M. Martin, "Demonstration of a low-noise near-infrared photon counter with multiphoton discrimination," *Nature Photon.*, vol. 83, p. 791, 2003.

[38] E. Waks, K. Inoue, W. D. Oliver, E. Diamanti, and Y. Yamamoto, "High-efficiency photon-number detection for quantum information processing," *IEEE Journal of Selected Topics in Quantum Electronics*, vol. 9, pp. 1502–1511, Nov 2003.

[39] K. Yamamoto, K. Yamamura, K. Sato, T. Ota, H. Suzuki, and S. Ohsuka, "Development of multi-pixel photon counter (mppc)," *IEEE Nucl. Sci. Symp. Conf. Record*, vol. 2, pp. 1094–1097, 2006.

[40] L. A. Jiang, E. A. Dauler, and J. T. Chang, "Photon-number-resolving detector with 10 bits of resolution," *Phys. Rev. A*, vol. 75, p. 062325, Jun 2007.

[41] D. Achilles, C. Silberhorn, C. Śliwa, K. Banaszek, and I. A. Walmsley, "Fiber-assisted detection with photon number resolution," *Opt. Lett.*, vol. 28, pp. 2387–2389, Dec 2003.

[42] M. J. Fitch, B. C. Jacobs, T. B. Pittman, and J. D. Franson, "Photon-number resolution using time-multiplexed single-photon detectors," *Phys. Rev. A*, vol. 68, p. 043814, Oct 2003.

[43] D. Achilles, C. Silberhorn, and I. A. Walmsley, "Direct, loss-tolerant characterization of nonclassical photon statistics," *Phys. Rev. Lett.*, vol. 97, p. 043602, Jul 2006.

[44] G. Zambra, M. Bondani, A. S. Spinelli, F. Paleari, and A. Andreoni *Rev. Sci. Instrum.*, vol. 75, pp. 2762–2765, 2004.

[45] B. E. Kardynal, Z. L. Yuan, and A. J. Shields, "An avalanche-photodiode-based photon-number-resolving detector," *Nature Photonics*, vol. 2, p. 425, 2008.

[46] K. Banaszek and I. A. Walmsley, "Photon counting with a loop detector," *Opt. Lett.*, vol. 28, pp. 52–54, Jan 2003.

[47] A. Divochiy, F. Marsili, D. Bitauld, A. Gaggero, R. Leoni, F. Mattioli, A. Korneev, V. Seleznev, N. Kaurova, O. Minaeva, G. Gol'tsman, K. G. Lagoudakis, M. Benkhaoul, F. Lévy, and A. Fiore, "Superconducting nanowire photon-number-resolving detector at telecommunication wavelengths," *Nature Photonics*, vol. 2, pp. 302–306, 2008.

[48] F. Marsili, D. Bitauld, A. Gaggero, S. Jahanmirinejad, R. Leoni, F. Mattioli, and A. Fiore, "Physics and application of photon number resolving detectors based on superconducting parallel nanowires," *New J. Phys.*, vol. 11, p. 045022, 2009.

[49] Z. Zhou, U. Vogl, R. T. Glasser, Z. Qin, Y. Fang, J. Jing, and W. Zhang, "Characterizing micro-macro transitions with an atomic-vapor-based linear optical amplifier," 2016.

[50] S. M. Barnett and P. L. Knight, "Thermofield analysis of squeezing and statistical mixtures in quantum optics," *J. Opt. Soc. Am. B*, vol. 2, pp. 467–479, 1985.

[51] B. Yurke and M. Potasek, "Obtainment of thermal noise from a pure quantum state," *Phys. Rev. A*, vol. 36, pp. 3464–3466, Oct 1987.

[52] S. M. Barnett and P. L. Knight, "Comment on "obtainment of thermal noise from a pure quantum state"," *Phys. Rev. A*, vol. 38, pp. 1657–1658, Aug 1988.

[53] R. E. Slusher, L. W. Hollberg, B. Yurke, J. C. Mertz, and J. F. Valley, "Observation of squeezed states generated by four-wave mixing in an optical cavity," *Phys. Rev. Lett.*, vol. 55, pp. 2409–2412, Nov 1985.

[54] P. M. Anisimov, G. M. Raterman, A. Chiruvelli, W. N. Plick, S. D. Huver, H. Lee, and J. P. Dowling, "Quantum metrology with two-mode squeezed vacuum: Parity detection beats the heisenberg limit," *Phys. Rev. Lett.*, vol. 104, p. 103602, Mar 2010.

[55] Z. Huang, K. R. Motes, P. M. Anisimov, J. P. Dowling, and D. W. Berry, "Adaptive phase estimation with two-mode squeezed vacuum and parity measurement," *Phys. Rev. A*, vol. 95, p. 053837, May 2017.

[56] P. T. Cochrane, G. J. Milburn, and W. J. Munro, "Teleportation using coupled oscillator states," *Phys. Rev. A*, vol. 62, p. 062307, Nov 2000.

[57] V. H. Tobias Eberle and R. Schnabel, "Stable control of 10 db two-mode squeezed vacuum states of light," *Optic Express*, vol. 21, pp. 11546–11553, 2013.

[58] A. I. Lvovsky, *Squeezed Light*, ch. 5, pp. 121–163. John Wiley Sons, Ltd, 2015.

[59] D. F. Walls and G. J. Milburn, *Quantum Optics*. Springer-Verlag, 2008.

[60] B. T. Gard, *Advances in Quantum Metrology: Continuous Variables in Phase Space*. PhD thesis, Louisiana State University, 2016.

[61] S. Khatri and N. Lütkenhaus, "Numerical evidence for bound secrecy from two-way post-processing in quantum key distribution," *Phys. Rev. A*, vol. 95, p. 042320, Apr 2017.

[62] D. F. V. James and P. G. Kwiat, "Atomic-vapor-based high efficiency optical detectors with photon number resolution," *Phys. Rev. Lett.*, vol. 89, p. 183601, Oct 2002.

[63] A. Imamo ̄glu, "High efficiency photon counting using stored light," *Phys. Rev. Lett.*, vol. 89, p. 163602, Sep 2002.

[64] M. A. Rowe, D. Kielpinski, V. Meyer, C. A. Sackett, W. M. Itano, C. Monroe, and D. J. Wineland, "Experimental violation of a bell's inequality with efficient detection," *Nature*, vol. 409, pp. 791–794, 2001.

[65] K.-J. Boller, A. Imamoğlu, and S. E. Harris, "Observation of electromagnetically induced transparency," *Phys. Rev. Lett.*, vol. 66, pp. 2593–2596, May 1991.

[66] M. D. Lukin and A. Imamoğlu, "Observation of electromagnetically induced transparency," *Nature*, vol. 413, pp. 273–276, Sep 2001.

[67] N. S. C. Clausen and M. Drewsen, "Analysis of a photon number resolving detector based on fluorescence readout of an ion coulomb crystal quantum memory inside an optical cavity," *New Journal of Physics*, vol. 15, p. 025021, 2013.

[68] M. A. Bouchiat and J. Brossel, "Relaxation of optically pumped rb atoms on paraffin-coated walls," *Phys. Rev.*, vol. 147, pp. 41–54, Jul 1966.

[69] M. T. Graf, D. F. Kimball, S. M. Rochester, K. Kerner, C. Wong, D. Budker, E. B. Alexandrov, M. V. Balabas, and V. V. Yashchuk, "Relaxation of atomic polarization in paraffin-coated cesium vapor cells," *Phys. Rev. A*, vol. 72, p. 023401, Aug 2005.

[70] W. Franzen, "Spin relaxation of optically aligned rubidium vapor," *Phys. Rev.*, vol. 115, pp. 850–856, Aug 1959.

[71] D. A. Steck, *Alkali D Line Data*.

[72] U. Gaubatz, P. Rudecki, S. Schiemann, and K. Bergmann, "Population transfer between molecular vibrational levels by stimulated raman scattering with partially overlapping laser fields. a new concept and experimental results," *The Journal of Chemical Physics*, vol. 92, no. 9, pp. 5363–5376, 1990.

[73] P. Marte, P. Zoller, and J. L. Hall, "Coherent atomic mirrors and beam splitters by adiabatic passage in multilevel systems," *Phys. Rev. A*, vol. 44, pp. R4118–R4121, Oct 1991.

[74] E. Talebian, "A short review note on the qubits and swap," *Optik*, vol. 124, no. 20, pp. 4400 – 4401, 2013.

[75] B. Klaas, N. Hanns-Christoph, P. Cristian, G. Gerald, M. Eduard, Q. Martin, S. Georg, W. Gunther, O. Silke, K. Axel, L. Stefano, S. Alexander, P. Pirro, H. Burkard, Z. Xue-Feng, Z. Jie, D. Michael, K. H. Winfried, W. Sebastian, H. Thomas, W. Hai-Lin, S. P. Gheorghe, V. V. Nikolay, M. Jordi, B. Thomas, J. B. Timothy, D. G. David, W. F. Robert, G. R. Mark, N. Edvardas, A. Marcis, B. Dmitry, P. Adriana, and H. K. Christoph, "Roadmap on STIRAP applications," *Journal of Physics B: Atomic, Molecular and Optical Physics*, vol. 52, p. 202001, sep 2019.

[76] Z. Kis and F. Renzoni, "Qubit rotation by stimulated raman adiabatic passage," *Phys. Rev. A*, vol. 65, p. 032318, Feb 2002.

[77] N. V. Vitanov, A. A. Rangelov, B. W. Shore, and K. Bergmann, "Stimulated raman adiabatic passage in physics, chemistry, and beyond," *Rev. Mod. Phys.*, vol. 89, p. 015006, Mar 2017.

[78] M. Fleischhauer, A. Imamoglu, and J. P. Marangos, "Electromagnetically induced transparency: Optics in coherent media," *Rev. Mod. Phys.*, vol. 77, pp. 633–673, Jul 2005.

[79] M. S. Feld and A. Javan, "Laser-induced line-narrowing effects in coupled doppler-broadened transitions," *Phys. Rev.*, vol. 177, pp. 540–562, Jan 1969.

[80] B. W. Shore, "Picturing stimulated raman adiabatic passage: a stirap tutorial,"*Adv. Opt. Photon.*, vol. 9, pp. 563–719, Sep 2017.

[81] N. V. Vitanov, K.-A. Suominen, and B. W. Shore, "Creation of coherent atomic superpositions by fractional stimulated raman adiabatic passage," *Journal of Physics B: Atomic, Molecular and Optical Physics*, vol. 32, pp. 4535–4546, Sep 1999.

[82] D. Daems and S. Guérin, "Adiabatic quantum search scheme with atoms in a cavity driven by lasers," *Phys. Rev. Lett.*, vol. 99, p. 170503, Oct 2007.

[83] J. S. Massa, A. M. Wallace, G. S. Buller, S. J. Fancey, and A. C. Walker, "Laser depth measurement based on time-correlated single-photon counting," *Opt. Lett.*, vol. 22, pp. 543–545, Apr 1997.

[84] G.Buller and A. Wallace, "Ranging and three-dimensional imaging using time-correlated single-photon counting and point-by-point acquisition," *IEEE Journal of Selected Topics in Quantum Electronics*, vol. 13, pp. 1006–1015, July 2007.

[85] B. Schwarz, "Mapping the world in 3d," *Nature Photonics*, vol. 4, no. 7, pp. 429–430, 2010.

[86] C. L. Glennie, W. E. Carter, R. L. Shrestha, and W. E. Dietrich, "Geodetic imaging with airborne LiDAR: the earths surface revealed," *Reports on Progress in Physics*, vol. 76, p. 086801, jul 2013.

[87] A. McCarthy, R. J. Collins, N. J. Krichel, V. Fernández, A. M. Wallace, and G. S. Buller, "Long-range time-of-flight scanning sensor based on high-speed time-correlated single-photon counting," *Appl. Opt.*, vol. 48, pp. 6241–6251, Nov 2009.

[88] R. E. Warburton, A. McCarthy, A. M. Wallace, S. Hernandez-Marin, R. H. Hadfield, S. W. Nam, and G. S. Buller, "Subcentimeter depth resolution using a single-photon counting time-of-flight laser ranging system at 1550 nm wavelength," *Optics letters*, vol. 32, no. 15, pp. 2266–2268, 2007.

[89] G. A. Howland, D. J. Lum, M. R. Ware, and J. C. Howell, "Photon counting compressive depth mapping," *Optics express*, vol. 21, no. 20, pp. 23822–23837, 2013.

[90] A. M. Pawlikowska, A. Halimi, R. A. Lamb, and G. S. Buller, "Single-photon three-dimensional imaging at up to 10 kilometers range," *Optics express*, vol. 25, no. 10, pp. 11919–11931, 2017.

[91] Z.-P. Li, X. Huang, Y. Cao, B. Wang, Y.-H. Li, W. Jin, C. Yu, J. Zhang, Q. Zhang, C.-Z. Peng, *et al.*, "Single-photon computational 3d imaging at 45 km," *arXiv preprint arXiv:1904.10341*, 2019.

[92] Z. Bao, Y. Liang, Z. Wang, Z. Li, E. Wu, G. Wu, and H. Zeng, "Laser ranging at few-photon level by photon-number-resolving detection," *Applied optics*, vol. 53, no. 18, pp. 3908–3912, 2014.

[93] Y. Sher, L. Cohen, D. Istrati, and H. S. Eisenberg, "Low intensity lidar using compressed sensing and a photon number resolving detector," in *Emerging Digital Micromirror Device Based Systems and Applications X*, vol. 10546, p. 105460J, International Society for Optics and Photonics, 2018.

[94] U. Dorner, R. Demkowicz-Dobrzanski, B. Smith, J. Lundeen, W. Wasilewski, K. Banaszek, and I. Walmsley, "Optimal quantum phase estimation," *Physical review letters*, vol. 102, no. 4, p. 040403, 2009.

[95] T.-W. Lee, S. D. Huver, H. Lee, L. Kaplan, S. B. McCracken, C. Min, D. B. Uskov, C. F. Wildfeuer, G. Veronis, and J. P. Dowling, "Optimization of quantum interferometric metrological sensors in the presence of photon loss," *Physical Review A*, vol. 80, no. 6, p. 063803, 2009.

[96] X.-F. Qian, B. Little, J. C. Howell, and J. Eberly, "Shifting the quantum-classical boundary: theory and experiment for statistically classical optical fields," *Optica*, vol. 2, no. 7, pp. 611–615, 2015.

[97] M. Giustina, A. Mech, S. Ramelow, B. Wittmann, J. Kofler, J. Beyer, A. Lita, B. Calkins, T. Gerrits, S. W. Nam, *et al.*, "Bell violation using entangled photons without the fair-sampling assumption," *Nature*, vol. 497, no. 7448, p. 227, 2013.

[98] J. S. Bell, "Speakable and unspeakable in quantum mechanics," *Cambridge University*, 1987.

[99] J. Busck and H. Heiselberg, "Gated viewing and high-accuracy three-dimensional laser radar," *Applied optics*, vol. 43, no. 24, pp. 4705–4710, 2004.

[100] L. Dovrat, M. Bakstein, D. Istrati, A. Shaham, and H. S. Eisenberg, "Measurements of the dependence of the photon-number distribution on the number of modes in parametric down-conversion," *Optics express*, vol. 20, no. 3, pp. 2266–2276, 2012.

[101] J. Aasi, J. Abadie, B. Abbott, R. Abbott, T. Abbott, M. Abernathy, C. Adams, T. Adams, P. Addesso, R. Adhikari, *et al.*, "Enhanced sensitivity of the ligo gravitational wave detector by using squeezed states of light," *Nature Photonics*, vol. 7, no. 8, p. 613, 2013.

[102] Y. Israel, S. Rosen, and Y. Silberberg, "Supersensitive polarization microscopy using noon states of light," *Physical review letters*, vol. 112, no. 10, p. 103604, 2014.

[103] B. Escher, R. de Matos Filho, and L. Davidovich, "General framework for estimating the ultimate precision limit in noisy quantum-enhanced metrology," *Nature Physics*, vol. 7, no. 5, p. 406, 2011.

[104] L. Cohen, Y. Pilnyak, D. Istrati, A. Retzker, and H. S. Eisenberg, "Demonstration of a quantum error correction for enhanced sensitivity of photonic measurements," *Physical Review A*, vol. 94, no. 1, p. 012324, 2016.

[105] L. Cohen, Y. Pilnyak, D. Istrati, N. M. Studer, J. P. Dowling, and H. S. Eisenberg, "Absolute calibration of single-photon and multiplexed photon-number-resolving detectors," *Physical Review A*, vol. 98, no. 1, p. 013811, 2018.

[106] G. Khoury, H. S. Eisenberg, E. Fonseca, and D. Bouwmeester, "Nonlinear interferometry via fock-state projection," *Physical review letters*, vol. 96, no. 20, p. 203601, 2006.

[107] V. C. Coffey, "Integrated lidar transforming transportation," *Optics and Photonics News*, vol. 30, no. 09, pp. 42–47, 2019.

[108] K. Hamamatsu Photonics, "Mppc® (multi-pixel photon counter) - s13360 series." (Accessed: 10 March 2019).

[109] K. Hamamatsu Photonics, "Photocathode technology:elemental technology hamamatsu photonics." (Accessed: 19 February 2019).

[110] L. Dovrat, M. Bakstein, D. Istrati, and H. S. Eisenberg, "Simulations of photon detection in silicon photomultiplier number-resolving detectors," *Physica Scripta*, vol. 2012, no. T147, p. 014010, 2012.

[111] M. Fox, *Quantum optics: an introduction*, vol. 15. OUP Oxford, 2006.

VITA

Elisha Siddiqui Matekole was born and raised in Delhi, India. She completed her high school at Presentation Convent Sr. Sec. School, Delhi. Subsequently she graduated with honors in Physics from St. Stephen's College, Delhi University. She completed her masters in Physics from Jawahar Lal Nehru University, Delhi. In the fall of 2013, Elisha arrived at Louisiana State University to pursue her Ph.D in Physics. After completing her M.S. in computational condensed matter Physics, she joined the Quantum science and technology group at LSU where she worked with Dr. Jonathan P. Dowling and Dr. Hwang Lee. Elisha met her husband in the choir at The Chapel on campus at LSU, and got married at the Baton Rouge Botanical gardens. In her spare time she enjoys learning music and reading. She loves listening to apologetic talks, and experimenting with healthy but delicious baking.

Author's Publications

Refereed Journal Articles

Published

- Room-temperature photon-number-resolved detection using a two-mode squeezer By: Elisha S. Matekole, Deepti Vaidyanathan, Kenji W. Arai, Ryan T. Glasser, Hwang Lee, and Jonathan P. Dowling, Physical Review A 96, 053815, Published 7 November 2017.
- Limits to Atom Vapor Based Room-Temperature Photon Number Resolving Detection By: Elisha S. Matekole, Hwang Lee, Jonathan P. Dowling, Phys. Rev. A 98, 033829, Published 28 September 2018.
- Sub-shot-noise-limited phase estimation via SU(1,1) interferometer with thermal states By: Xiaoping Ma, Chenglong You, Sushovit Adhikari, Elisha S. Matekole, Hwang Lee, and Jonathan P. Dowling, Opt. Express 26, 18492-18504 (2018).
- Thresholded Quantum LIDAR — Exploiting Photon-Number-Resolving Detection By: L. Cohen, Elisha S. Matekole, Y. Sher, D. Istrati, H. S. Eisenberg, J. P. Dowling, Phys. Rev.

Lett. 123, 203601, (2019).

- Quantum interference between light sources separated by 150 million kilometers By:Yu-Hao Deng, Hui Wang, Xing Ding, Z.-C. Duan, Jian Qin, M.-C. Chen, Yu He, Yu-Ming He, Jin-Peng Li, Yu-Huai Li, Li-Chao Peng, E. S. Matekole, Tim Byrnes, C. Schneider, M. Kamp, Da-Wei Wang, Jonathan P. Dowling, Sven Höfling, Chao-Yang Lu, Marlan O. Scully, Jian-Wei Pan. Research in collaboration with the University of Science and Technology of China, Shanghai, and NYU, Shanghai Phys. Rev. Lett. 123, 080401, (2019).

In preparation

- Squeezed Light Detection Using Camera, Elisha S. Matekole, L. Cohen, S. Cuzzo, Narayan Bhushal, H. Lee, E. Mikhailov, I. Novikova, J. P. Dowling.

- Optical gyroscope with coherence-boosted two-mode squeezed beams, Xiao-Qi Xiao, Elisha S. Matekole, Jiankang Zhao, Guihua Zeng, Jonathan P.Dowling, and Hwang Lee.